Award number: DE-SC0018967

Final Technical Report

High concentrations of ice: investigations using polarimetric radar observations combined with in situ measurements and cloud modeling

Principal Investigators:

Dr. Alexander Ryzhkov, University of Oklahoma, USA

Dr. Alexander Khain, The Hebrew University of Jerusalem, Israel

Dr. Vaughan Phillips, Lund University, Sweden

Table of Contents **pp**

I. Modeling studies at Lund University

1.1. Introduction

Number concentrations of ice in cold clouds are influential for their properties and extent, and hence for the climate. A variety of mechanisms exist for initiation of ice in cold clouds. Primary ice production involves nucleation of ice by either solid aerosols acting heterogeneously as ice-nucleating particles (INPs), (e.g., Fletcher 1962), or by cloud-droplets freezing homogeneously. Such droplets are from solute aerosols acting as cloud condensation nuclei (CCN). Secondary ice production (SIP) involves fragmentation somehow of precipitation. Many mechanisms of SIP are known from laboratory studies (reviewed by Pruppacher and Klett 1997; Cantrell and Heymsfield 2005; Field *et al*. 2017), including:

- Rime-splintering between -3 and -8 ºC (Hallett and Mossop 1974);
- Fragmentation of freezing raindrops or drizzle (Johnson and Hallett 1968; Takahashi and Yamashita 1977);
- Breakup in ice-ice collisions (Vardiman 1978; Takahashi *et al.* 1995);
- Breakup during sublimation (Oraltay and Hallett 1989; Dong *et al.* 1994).

Observations by aircraft of cold clouds too warm for homogeneous freezing (near -36 ºC) have revealed high concentrations of ice particles. They can exceed concentrations of active INPs by 3 or 4 orders of magnitude. Hobbs *et al*. (1980) quantified this excess by the ice enhancement (IE) ratio in ascending convective cloud tops sampled over the continental USA. A trend of decreasing IE ratio with decreasing cloud-top temperature was observed. While measurement biases were discovered more recently (e.g., Field *et al.* 2006; Korolev *et al*. 2011), a similar excess has been seen in modern campaigns without such biases (e.g. Lawson *et al.* 2015; Lasher-Trapp *et al.* 2016, 2021; Fridlind *et al*. 2017).

There has been progress recently. Representing all four known SIP mechanisms noted above, Waman *et al.* (2022) predicted with a cloud-resolving model the observed order of magnitude of IE ratio reported in cloud-top regions by Hobbs *et al*. (1980), along with its general trend with cloud-top temperature. Also, Huang *et al.* (2022) correctly predicted observed ice concentrations with a cloud model representing some of these SIP mechanisms for tropical maritime deep convection.

In the upper troposphere, clouds with homogeneous freezing from tops above the -36 ºC level have also shown high concentrations of ice (Rosenfeld and Woodley 2000). Ice concentrations were seen with orders of magnitude similar to those of supercooled cloud-droplets in convective updrafts. However, there are still uncertainties, for example, concerning the role of preferential evaporation of smaller droplets during homogeneous freezing.

There is a need to understand the reasons for high concentrations of ice in clouds, since their glaciation influences precipitation globally. There are two possible mechanisms for precipitation, one involving the vapour growth of ice crystals with later aggregation (clumping together of

crystals) and riming (accretion of supercooled cloud-liquid), with possible melting to form 'cold rain'. The other involves coalescence of cloud-droplets to form 'warm rain'. Outside the tropics over land, depending on the aerosol conditions, cold rain appears to prevail, although there is uncertainty (Field and Heymsfield 2015). There, the cloud-base is not warm enough for cloud-droplets to be large enough aloft for coalescence.

Another reason for studying ice initiation is that cold clouds influence climate change. Mixed-phase clouds globally exert a radiative forcing of about 4 W m^{-2} (Matus and L'Ecuyer 2017), which is similar to the radiative forcing from instantaneous doubling of CO2 in the atmosphere. Mixed-phase clouds involve SIP and must have an even greater impact than 4 W m^{-2} on the Earth's radiation budget since convective outflow is a major source of ice-only layer-cloud. When the ascent is reduced, the cloud-liquid evaporates, rendering a cloud ice-only, while the ice particles initiated in the original mixed-phase cloud persist. According to the Intergovernmental Panel on Climate Change (IPCC) (Soloman *et al*. 2007), anthropogenic aerosols are a major forcing for climate change. Microphysical and optical properties of clouds are altered by the changes in the loading and composition of aerosol particles from emissions. This influences the Earth's radiation budget by 'aerosol indirect effects' (Lohmann and Feichter 2005). Those effects involving glaciated clouds are the most uncertain.

Consequently, the present 3-year project has aimed to explore reasons for high concentrations of ice being produced in clouds. The role of the Lund side has been to implement processes of ice nucleation and multiplication (*via* ice–ice collisions and drop freezing) in the spectral bin models. Mesoscale cloud systems have been simulated with an '*aerosol-cloud model*' (AC) created by Phillips. AC is a Cloud-System Resolving Model (CSRM) with 2-moment bulk/emulated bin microphysics and about a dozen aerosol species, as described by Phillips *et al.* (2009, 2013, 2014, 2015ab, 2017ab, 2018, 2020). AC was updated to resolve 5 types of primary bioaerosols with a new scheme based on field observations in Amazonia (Patade *et al.* 2021) and an overlooked mechanism of breakup of ice during sublimation (Deshmukh *et al.* 2022; Waman *et al.* 2022). The approach was to simulate an observed storm case from a past DoE-funded field campaign, comparing the simulation with coincident aircraft observations.

During the project on the Lund side, a specific hypothesis was tested, namely that SIP could determine the observed multi-polarimetric radar properties and influence cloud properties more than the ice nucleating particles (INPs). To that end, we performed a modeling study altering the concentrations of primary biological aerosol particles (PBAPs).

The report is structured as follows. In the next section, the project objectives for the Lund side and their completion are described. The published papers are documented. In the concluding section, corresponding discoveries in the project are outline.

1.2. Summary of Progress During Project

1.2.1 Objectives of the Overall Project led by OU

In Year 1, Phillips began work on studying the role of SIP for charge separation and its dependency on updraft speeds and aerosol conditions. A cold-based multi-cell convective storm observed in a field campaign (STEPS) two decades ago was simulated with a mesoscale 3D model (domain about 100 km wide). Results were submitted in a two-part paper (Phillips *et al.* 2020, 2022) in Year 1. In Years 2 and 3, the paper was revised. Both parts are now finally published and support is acknowledged for the subaward to Lund from Oklahoma University.

For the wider project led by Oklahoma University (OU), the objectives from the original proposal were:

I. Identify "*aircraft datasets suitable for analysis from the four field campaigns: MC3E…*" and *process "in situ aircraft data for selected events*".

II. Compare "*vertical profiles of IWC* [ice water content]*, Dm* [mean size]*, and Nt* [hydrometeor total number concentration] *retrieved from the polarimetric radar data … to identify the issues with the model"*;

III. Generate Columnar Vertical Profiles (CVPs*) "of polarimetric variables and parameters of size distribution of ice in the vertical columns following the aircraft tracks…*".

IV. Compare "*CVP ice retrievals with direct in situ aircraft measurements and refining the retrieval methodology.*"

V. Implement *modifications in "models to account for the processes of homogeneous nucleation and ice multiplication and realistic representation of the vertical profiles of microphysical parameters of ice.*"

VI. Examine "*CVP retrievals in different parts of the storms and creating climatology of the vertical profiles of size distribution parameters of ice with a focus on the difference between continental midlatitude and tropical systems.*"

VII. Optimise "*treatment of ice microphysical processes in the 2D HUCM and 3D WRF/SBM* [spectral bin microphysics] *models via interactive comparison of the model output and polarimetric radar retrievals."*

VIII. Recommend *"microphysical parameterization of ice processes in bulk models based on the outcome of this study."*

Phillips contributed directly to performing Objectives II, V, VII and VIII. Phillips assisted HUJ with achieving Objective V by informing them of changes to the codes of raindrop-freezing fragmentation and ice-ice collisional breakup. Phillips advised the HUJI side about new codes for HUCM (SBM), the chief model of the project, and renewed AC's treatment of ice multiplication. In summary, Phillips improved the cloud models of the project, enhancing OU's accomplishment of Objectives I−VIII.

1.2.2 Specific Objectives for Lund Side of Project

It was agreed with US Department of Energy (DoE) and OU to support a postdoctoral scholar to perform these objectives during Year 3 (annual report in 2020), to assist with Objective V of the wider project (Sec. 2.1):

1) Improve "*representations of ice nucleation and multiplication processes (via ice collisions and drop freezing) … for HUCM and AC"*;
2) Validate "*simulations of clouds observed in DoE field campaigns … against flight data*";
3) "*Assess further the role of primary and secondary ice production in creating high concentrations of ice in natural clouds*".

During Years 3 and 4 of the project, Objectives 1−3 were completed by Phillips at Lund.

1.2.3 Approach

During the project, our general approach for understanding the causes of high concentrations of ice in clouds has been to first upgrade the models using published lab results. Next, high-resolution simulations have been compared with field observations to establish accuracy and then analysed to evaluate the relative roles of various sources of ice particles. These simulations involve a mesoscale 3D domain that is about 100 km in width, with a resolution of about 2 km.

To achieve Objectives 1−3 on the Lund side and to assist OU with its Objectives I−VIII, such an approach was followed with this sequence of steps:

(a) Develop our cloud model (AC) further with implementation of extra types of INP (pollen, bacterial, algal, fungal, detritus), implement breakup during sublimation, and inclusion of tagging tracers, for example to track fragments from each type of SIP; and assist HUJ with development of HUCM to improve ice initation representations;
(b) Compare simulation with ground-based observations of precipitation, aircraft observations of liquid and ice properties, and multi-polarimetric observations of radar properties;
(c) Analyse validated simulation to see the contribution from various sources of ice using budgets and tagging tracers, and sensitivity tests;
(d) Predict multi-polarimetric radar signatures of SIP and compare with observations.

Regarding multi-polarimetric radar signatures, the specific differential phase (K_{DP}) was predicted by AC, in addition to the radar reflectivity (Z) and differential reflectivity (Z_{DR}). The advantage of K_{DP} is that it is more nearly sensitive to total number concentrations of dense ice particles. By contrast, Z is sensitive only to the largest ice particles present, which represent only a small fraction of the total number.

Our rationale is that cloud models with treatment of ice morphology can predict the signature patterns from such multi-polarimetric radar quantities due to any given type of SIP, in the phase-

space of their fundamental underlying variable. Such a signature (e.g., for K_{DP}) predicted for a few storm cases would assist in interpretation of radar observations of a wider variety of storms in future studies.

Another aspect of our rationale is that acuity of validation with many coincidently observed quantities allows confidence in the simulation. With AC, the approach is to validate the predicted CCN activity from observed loadings of various chemical species of aerosol, and quantities such as the surface precipitation, dynamics and microphysical properties of the cloud. Rigour of validation ensures, as far possible, that the correct results are predicted for the correct reasons, minimizing the chance of compensation between opposing biases among multiple cloud-related processes in the simulation.

1.2.4 Works Completed

The over-arching aim of the project was to compare the roles of various mechanisms of SIP, for multi-polarimetric radar properties and aircraft-observable cloud properties, in comparison with the effect from ice nucleating particles (INPs). To quantify the effect from INPs, for which many chemical species existing in the real atmosphere, we selected one broad INP type, namely bioaerosols. We improved the representation of PBAP-INPs by implementing a new scheme resolving its five types (Patade *et al.* 2021).

Tasks performed during the Years 3 and 4 of the project involved simulation of an observed case of a squall line over Oklahoma in USA from a DoE-funded field campaign. Predicted properties of cloud-microphysical species were studied following the approach outlined above (Sec. 1.2.3, steps (a)-(d)).

The results are described in publications in peer-reviewed journals (Sec. 1.2.5), chiefly in the paper by Patade *et al.* (2021). Phillips visited HUJ in Year 1 to assist with coding aspects of the ice multiplication in the HUCM (Sec. 1.2.1).

Discoveries from the Lund side of the project (Sec. 1.3) include the finding that K_{DP} is sensitive to inclusion of SIP by breakup in ice-ice collisions, especially in deep convection. Other discoveries relate to ice particle numbers from individual processes of ice initiation and the role of PBAPs as INPs.

In summary, objectives on the Lund side (Sec. 1.2.2) have been accomplished, as outlined below.

1.2.4.1 Objective 1: Improve representation of ice initiation in models

During the project (2018-2022), Phillips worked at Lund University on improving HUCM, and visited HUJ in November 2018. During the visit, Phillips created microphysical schemes and worked with HUJ staff to include them in HUCM, for these processes:

- ice multiplication by fragmentation in ice-ice collisions;

- homogeneous freezing of cloud-droplets, with a fraction of droplets that evaporate without freezing during ascent through the homogeneous freezing band of temperatures (about -35 to -38 ^{o}C).

The melting scheme was also discussed. Performance by the HUJ side of the project for Objectives I−VII in the overall project (Sec. 1.2.1) was thus assisted by Phillips.

During Year 4, a student supported on another funded project of Phillips analysed data from a portable probe for observing fragmentation in graupel-snow collisions. The probe was designed to be deployed on the ground during snowfall events. The student visited Vindeln in northern Sweden in February 2022. Video imagery of fragmentation of snowflakes falling into the probe was analysed to relate numbers of fragments to collision kinetic energy, for snow consisting of dendritic and non-dendritic crystal habits. In November 2022, a revised version of the scheme for breakup of snow in collisions with graupel/hail was applied in AC and is soon to be applied in HUCM.

1.2.4.2 Objective 2: Validate the model for observed storm case

A squall line moved over the ARM central facility (CF) on May 20, 2011, (11:00 to 14:00 UTC), in Oklahoma, USA, during the Mid-latitude Continental Convective Clouds Experiment (MC3E) campaign. It was sampled by the Citation aircraft. Vertical velocity is measured using the air motion sensing systems. In-cloud particle size distributions (PSDs) of cloud-particles and precipitation were measured with the Cloud Imaging Probe (CIP), a 2D Cloud Imaging Probe (2D-C), and the High-Volume Precipitation Spectrometer Probe (HVPS). Imagery from the 2D-C and CIP probes was processed with the algorithm from the National Center for Atmospheric Research (NCAR), reducing artefacts from shattering on the probes' outer edges (Field *et al.* 2006). The 2D-C probe had anti-shattering tips (Korolev *et al*. 2011). Also, a Cloud Droplet Probe (CDP) measured the PSD of cloud-droplets < 0.05 mm. Liquid water content (LWC) was measured by a King hot-wire probe.

Fig. 1.1 shows that the cloud-liquid properties are realistically predicted. Validated quantities include mean size of cloud-droplets and their number concentration, both for convective and stratiform regions separately. Fig. 1.2 shows adequate agreement between predicted and observed ice concentrations, with both differing by less than factors of about 2 and 4 in the convection and stratiform regions. There is good agreement too for the vertical profile of radar reflectivity and evolution of surface precipitation.

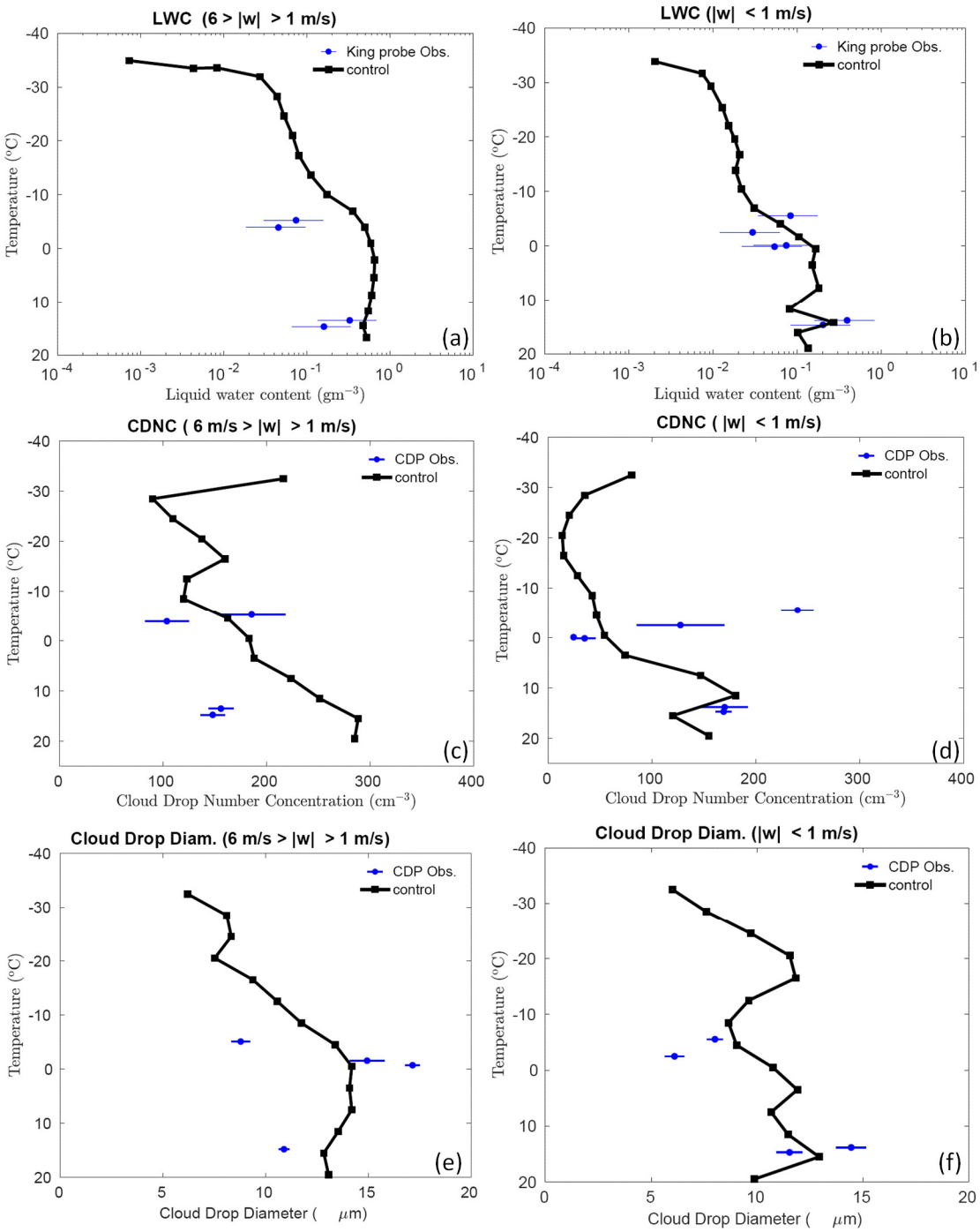

Fig. 1.1. *Comparison of the control simulations by AC with aircraft observations, for liquid water content averaged over (a) convective (*$1 < |w| < 6$ *m/s) and (b) stratiform (*$|w| < 1$ *m/s) regions; cloud drop number concentration over (c) convective and (d) stratiform regions; and the average size of cloud droplets (< 20 μm) conditionally averaged over (e) convective and (f) stratiform regions.*

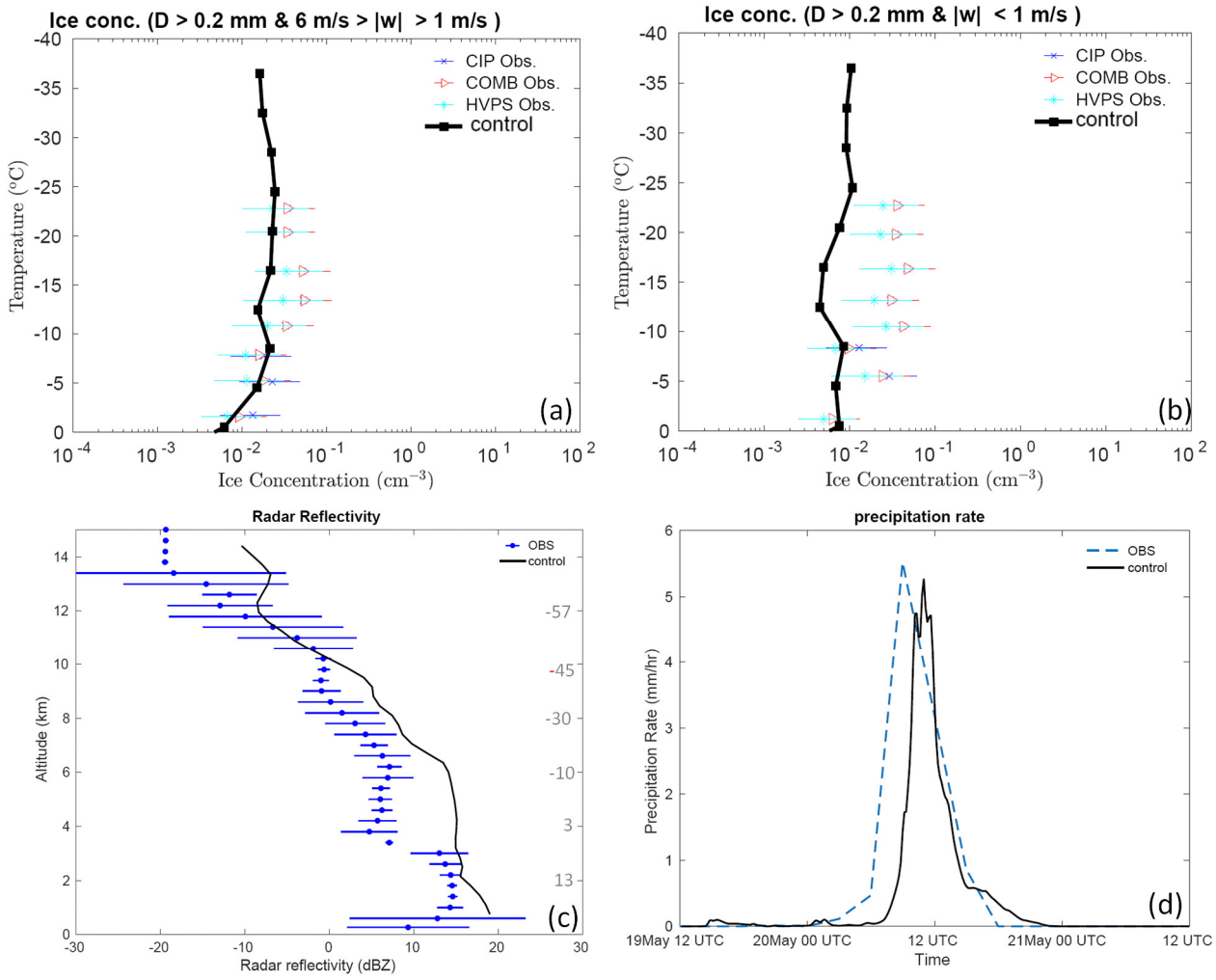

Fig. 1.2. *Comparison of the control simulations by AC with aircraft observations, for ice number concentration of all particles > 0.2 mm in the maximum dimension of all microphysical species (cloud ice, graupel/hail, snow), averaged over (a) convective (*$1 < |w| < 6$ *m/s) and (b) stratiform (*$|w| < 1$ *m/s) regions. (c) The vertical profile of simulated radar reflectivity conditionally averaged over all regions of significant reflectivity (*> -20 *dBZ) at each level is compared with observations from ground-based radars, with temperature on the right axis; and (d) predicted precipitation rate (mm/hr) compared with ground observations at the CF. From Patade et al. (2022).*

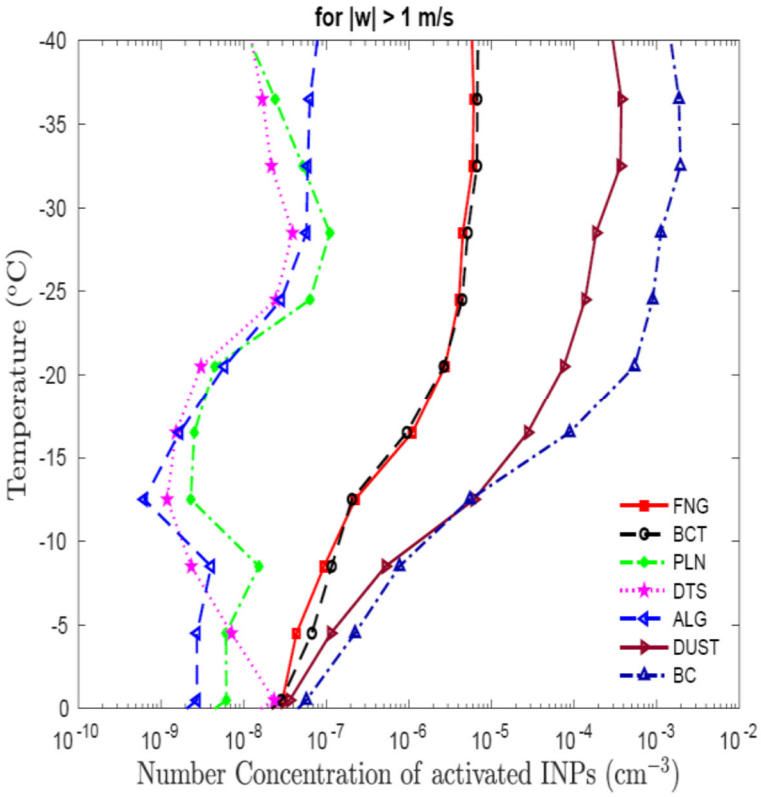

Fig. 1.3. *The activated number concentration of INPs from various PBAP groups along with dust (DUST) and black carbon (BC) at various temperatures for convective regions. These bioaerosol groups are 'FNG' for fungal particles, 'BCT' for bacterial particles, 'PLN' for pollen, 'DTS' for plant/animal detritus, and 'ALG' for algal particles. All the vertical profiles shown here are averaged for the whole domain, with temperature as a vertical coordinate. From Patade et al. (2022).*

1.2.4.3 Objective 3: Assess the roles of primary and secondary ice production

The validated 'control' simulation of the MC3E case (Sec. 2.4.2) was analysed for the contributions from various types of ice initiation. First, regarding primary ice nucleation, the contributions from the multiple species of INP were mapped out. These showed the soot and mineral dust were the most prolific INP types, with PBAP-INPs being at least an order of magnitude less abundant (Fig. 1.3). Fungal and bacterial PBAPs contribute the most to the biological ice nucleation.

Fig. 1.3 shows the budget of all ice particles initiated from various primary and secondary sources. Homogeneous freezing of supercooled cloud droplets dominates overall. Among all types of SIP, breakup caused by collisions between various ice particles prevails for the total ice number concentration (Fig. 1.4b). Although sublimation breakup of graupel seems almost as prolific as homogeneous freezing in the total ice concentration, most of the resulting fragments disappear by

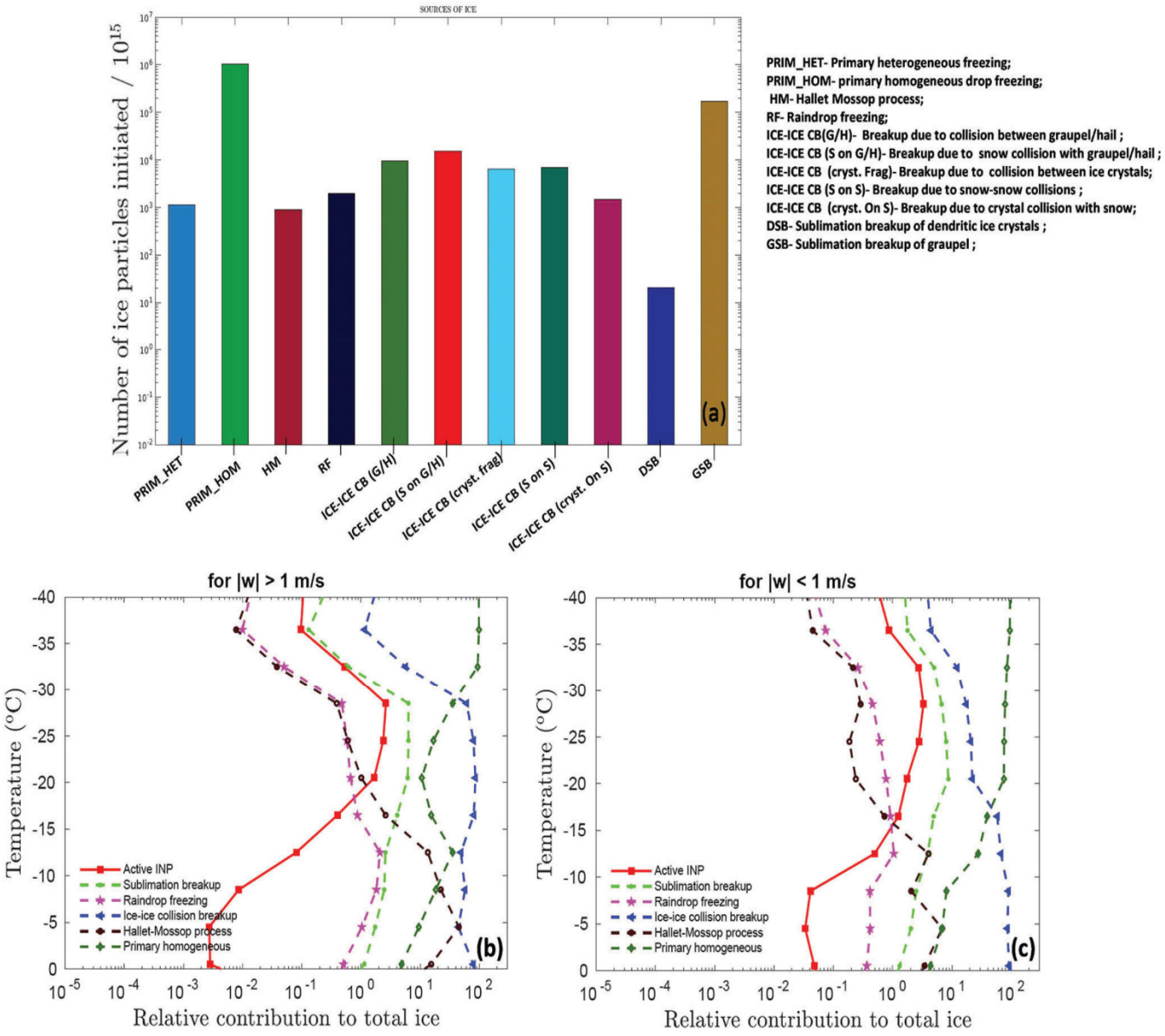

Fig. 1.4. *(a) the budget of numbers of ice particles initiated throughout the entire simulation from various sources. These include heterogeneous and homogeneous ice nucleation, as well as four mechanisms of SIP (H-M process, raindrop-freezing fragmentation, breakup in ice-ice collisions for permutations of microphysical species, and sublimational breakup). Also shown are the vertical profiles of the percentage relative contribution to the total ice from each source in (b) convective and (c) stratiform/cirriform regions. From Patade et al. (2022).*

sublimation in regions of descent soon after being produced. They are inconsequential. Yet a small and significant fraction of the fragments from sublimational breakup survive by somehow exiting the downdrafts. For example, they can be mixed into an adjacent mixed-phase updraft where they grow.

Fig. 1.4b,c reveals that overall the ice enhancement by ice multiplication (SIP), relative to the first ice from INPs, is about 10^2 in the middle of the mixed-phase region (0 to -36 ºC), (compare red and blue lines in **Fig. 4bc**). This ratio decreases with increasing height through the region, as reported by Hobbs *et al*. (1980). In both convective and stratiform regions, the average ice enhancement ratio (not shown here) decreases with increasing height from about 10^4 and 10^3 respectively near the freezing level to about 10^1 aloft (Patade *et al.* 2022).

Homogeneous freezing prevails in determining average concentrations of ice at levels above about -30 and -20 ºC in convective and stratiform regions respectively. Although it only occurs above the -36 ºC level, compensating subsidence, including convective downdrafts, brings it down into the mixed-phase region. In the lower half of the mixed-phase region in stratiform, and throughout most of this region in convection, only ice multiplication involving SIP can account for observed ice concentrations.

Fig. 1.4b,c elucidates the vertical distribution of the relative balance among SIP processes. While secondary ice particles at all levels are mostly dominated by breakup in ice-ice collisions, the lack of strong warmth of cloud-base and the high continental aerosol concentration combine to make mean droplet sizes too small for much coalescence, inhibiting raindrop-freezing fragmentation and the H-M process. So curiously, at most levels in the mixed-phase region, sublimational breakup is the second-most important SIP process.

Fig. 1.5 shows the sensitivity tests with respect exclusion of all SIP, only breakup in ice-ice collisions, and only breakup during sublimation. Exclusion of all SIP reduces the ice concentration by an order of magnitude at most levels below about -25 ºC in the convection, although there is a compensating response of supercooled cloud-liquid aloft and its homogeneous freezing. This lessens the apparent impact from SIP in the sensitivity test. Absence of breakup in ice-ice collisions approximately doubles the LWC in most of the mixed-phase region. Finally, sensitivity tests showed little effect from exclusion of sublimational breakup mostly.

K_{DP} was reduced by up to a factor of about 2 in the lower half of the mixed-phase region when all SIP was excluded (Fig. 1.5f). The compensating response boosted it by a similar factor at higher levels. Average K_{DP} over cloudy regions plotted on a phase-space of relative humidity with respect to ice (RHI) vs ice-bulb temperature, with and without sublimational breakup, revealed little effect (not shown). Yet a plot of average K_{DP} on a phase-space of vertical velocity and subzero ambient temperature showed a strong signature from inclusion of breakup in ice-ice collisions (Fig. 1.6). In moderate to strong convective updrafts (> 4 m/s), average K_{DP} is enhanced by this breakup by an order of magnitude at -30 ºC and by 0.5-1 orders of magnitude throughout the upper half of the mixed-phase region. But it is reduced by up to 0.5 orders of magnitude in weaker ascent ($<$ 4 m/s) and stratiform/cirriform cloud at such levels.

Finally, little impact from plausible fluctuations of PBAPs was found on properties of the simulated storm when extra sensitivity tests were performed. Simulations were compared with the control run with all PBAPs prohibited and with PBAP loadings increased by factors of 10, 100 and 1000 in the environment. Changes in the predicted average ice concentration were less than about

10% relative to the control for all runs, which was not significant. More details are given by Patade *et al.* (2022).

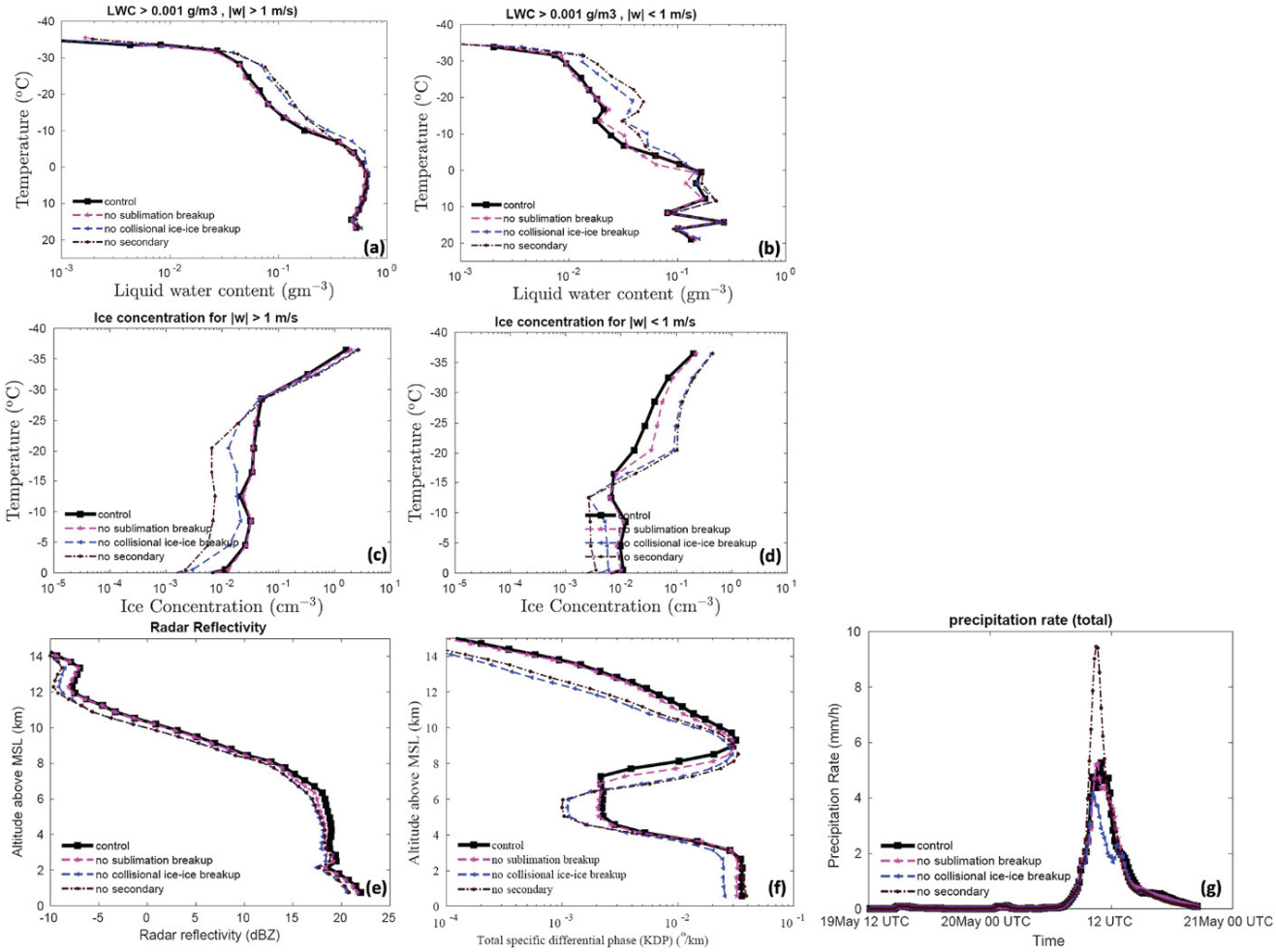

Fig. 1.5. *Temperature dependence of the liquid water content in (a) the convective and (b) the stratiform region for 'control' simulation and various sensitivity runs involving SIP mechanisms. The ice number concentration is also shown for the (c) convective and (d) stratiform regions. The averaging conditions are mentioned at the top of each figure. The vertical profiles of (e) radar reflectivity, (f) total specific differential phase ($\boldsymbol{K_{DP}}$) are also shown for the same simulations. (g) The temporal evolution of the total surface precipitation rate averaged over the domain is also shown. All the vertical profiles shown here are averaged for the whole domain. From Patade et al. (2022).*

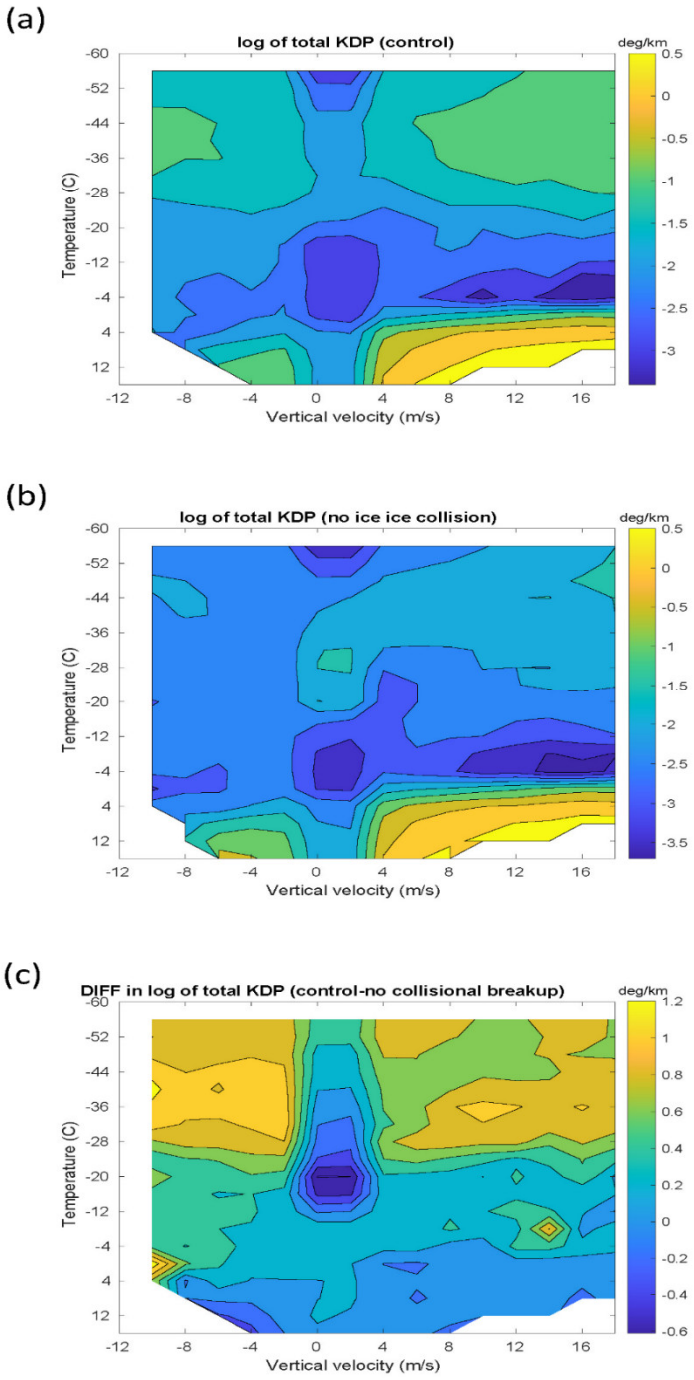

Fig. 1.6. *The logarithm (base 10) of total specific differential phase ($\boldsymbol{K_{DP}}$, deg/km) plotted on a phase-space of vertical velocity (m/s) and temperature (°C), for (a) the control simulation of MC3E (20 May 2011) and (b) the corresponding simulation without breakup in ice-ice collisions. Also shown in (c) is the difference of this logarithm of $\boldsymbol{K_{DP}}$ between (a) and (b).*

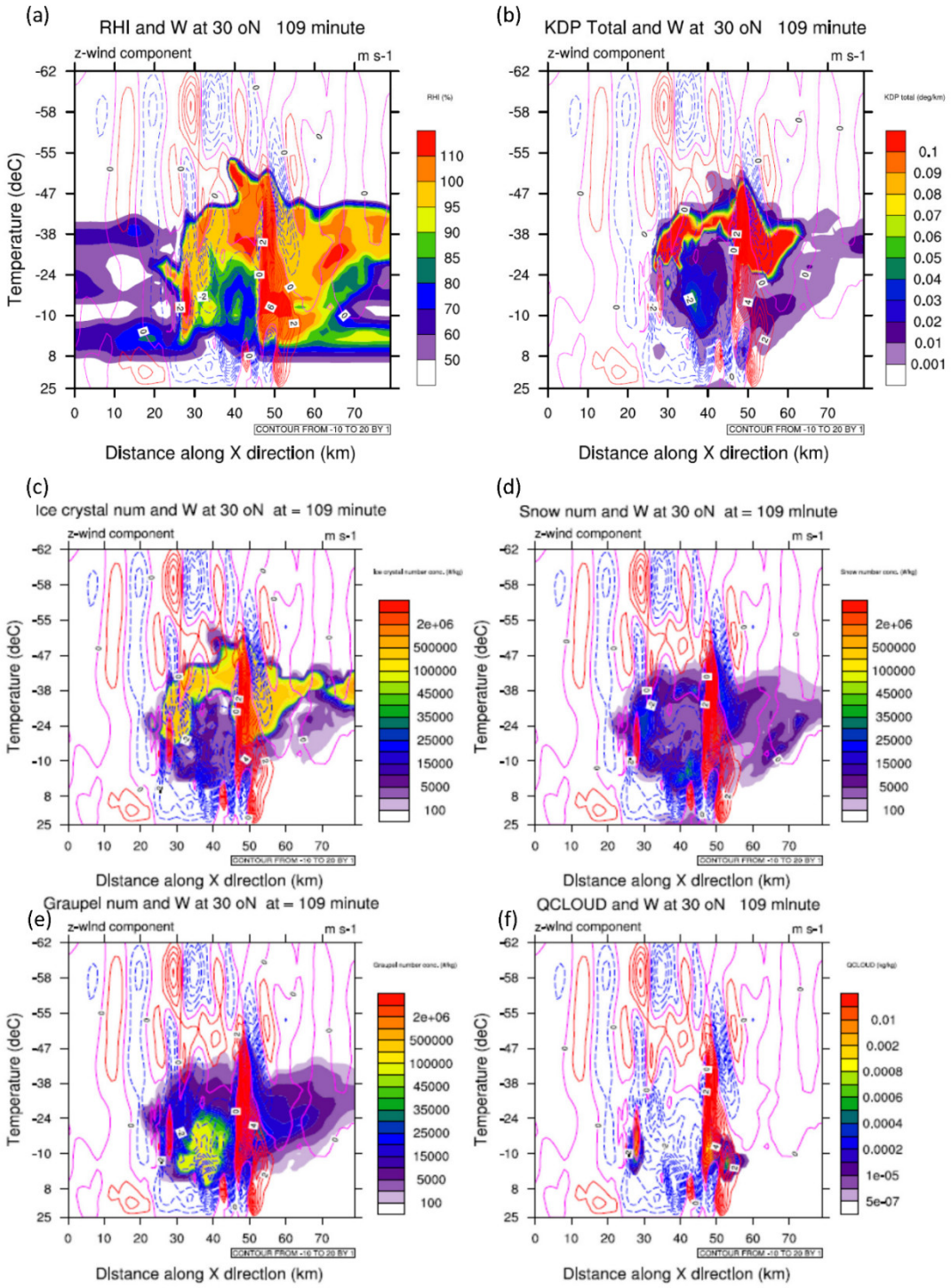

Fig. 1.7. *Various quantities on a vertical section through a convective cell in the mesoscale convective system from the control simulation. These are (a) relative humidity with respect to ice (RHI), (b) specific differential phase ($\boldsymbol{K_{DP}}$), number mixing ratios (#/kg) of (c) cloud-ice crystals, (d) snow and (e) graupel, and also (f) cloud-liquid mixing ratio (kg/kg). The vertical coordinate is temperature (^{o}C). Contours of vertical velocity are overlaid on all panels (red full lines for ascent, blue dashed lines for descent).*

Fig. 1.7 shows a snapshot of a thunderstorm cell from the control simulation at a certain time. K_{DP} is maximal in the region of ascent due to the abundance of ice precipitation there (e.g. snow), largely produced by accretion of cloud-liquid, which is restricted mostly to the convective updraft (> 1 m/s).

Homogeneously frozen ice prevails in the convective updraft above the -36 ºC level, and is downwelled by a kilometer or so around it in the compensating descent, at high concentrations (e.g., shaded orange). Sublimational breakup fragments are numerous in the convective downdraft (faster than about 1 m/s) at levels in the mixed-phase region where RHI is lower than 80% (e.g. shaded mauve around $x = 40$ km). Fragments from breakup in ice-ice collisions are ubiquitous at subzero levels (e.g. shaded yellow and orange), especially prevailing in the mixed-phase updraft (e.g. near $x = 47$ km).

The transient, turbulent-like, nature of the flow is reflected by the snapshot panels. This illustrates how sublimational breakup fragments can transfer from the convective downdraft into the updraft so that they then survive. This behavior is as theoretically predicted with a thought experiment and conceptual model by Deshmukh *et al.* (2022).

1.2.5 Products

This publication arose from work funded by the award of the present project, and was led by Phillips:

S. Patade, V. T. J. Phillips, D. Waman, A. Deshmukh, A. K. Gupta, A. Jadav, A. Bansemer, J. Carlin, and A. Ryzhkov: "The influence of multiple groups of biological ice nucleating particles on microphysical properties of mixed-phase clouds observed during MC3E", *Atmos. Chem. Phys*., **22**, 12055-12075 (2022)

Other publications about ice initiation were partly funded by the award of the present project (and partly also by a previous DoE award directly to Phillips):

V. T. J. Phillips, M. Formenton, L. Karlsson, V. Kanawade, J. Sun, C. Barthe, J.-P. Pinty, A. Detwiler, W. Lyu, and S. Tessendorf: "Multiple environmental Influences on the lightning of cold-based continental cumulonimbus clouds. Part I: description and validation of model", *J. Atmos. Sci*., **77**, 3999-4024 (2020)

V. T. J. Phillips, and S. Patade: "Multiple environmental influences on the lightning of cold-based continental cumulonimbus clouds. Part II: sensitivity tests for its charge structure and land-ocean contrast", *J. Atmos. Sci.*, **79,** 263–300 (2022)

A. Deshmukh, V. T. J. Phillips, A. Bansemer, S. Patade and D. Waman: "New empirical formulation for the sublimational breakup of graupel and dendritic snow", *J. Atmos. Sci*., **79,** 317-336 (2022)

D. Waman, A. Jadav, A. Deshmukh, V. T. J. Phillips, S. Patade, A. K. Gupta, A. Bansemer: "Dependencies of four mechanisms of secondary ice production on cloud top temperature in a continental convective storm", *J. Atmos. Sci.*, **79,** in press (2022)

X. Zhao, X. Liu, V. T. J. Phillips, and S. Patade: "Impacts of secondary ice production on Arctic mixed-phase clouds based on ARM observations and CAM6 single-column model simulations", *Atmos. Chem. Phys.,* **21**, 5685–5703 (2021)

This last paper by Zhao *et al.* (2021) has been the basis for subsequent global modeling assessments of SIP in the present-day climate (not involving the Lund side). Also, a paper has been submitted to a journal about the role of time-dependence of IN activity for cloud glaciation:

D. Waman, A. Deshmukh, A. Jadav, S. Patade, M. Gautam, V. T. J. Phillips, A. Bansemer, and J. Jakobsson: "Effects from time dependence of ice nucleus activity for contrasting cloud types", *J. Atmos. Sci*., in review (2022)

Support by DoE (ASR) *via* the subaward from University of Oklahoma is acknowledged in all of the above papers. Codes for the new process of ice initiation may be shared with US government laboratories and other institutions, freely on request.

1.3. Conclusions for section I.

During the project, the following conclusions were reached (Patade *et al.* 2022):

(1) PBAP-INPs have little impact on the microphysical, dynamical and radiative properties of a typical multi-cell convective storm (20 May 2011, MC3E), since they do not dominate the INP activity at most levels and other sources of ice are more prolific. This is true even when PBAP loadings are perturbed by a plausible factor that could occur in nature (e.g. 100 at all levels). Fungal and bacterial PBAPs contribute the most to the biological ice nucleation.

(2) The overall ice enhancement by SIP processes is by an IE ratio of about 10^3 at most levels. On average this ratio declines with height from about 10^3or 10^4 near the freezing level to about 10 aloft.

(3) Tagging tracers in the control simulation reveal that breakup in ice-ice collisions is the most prolific of the SIP mechanisms. In this particular storm case, the continental aerosol concentration and only moderate warmth of cloud-base combine to make mean droplet sizes too small for much coalescence, inhibiting raindrop-freezing fragmentation and the H-M process.

(4) Sublimational breakup by graupel in convective descent contributes weakly yet significantly to the overall ice enhancement in the control simulation (tagging tracers). This is especially so in convective downdrafts. It is generally the second-most important SIP mechanism after breakup in ice-ice collisions at most levels in the control run. Most of the fragments from sublimational breakup disappear by sublimation itself before they can enter

the updraft to grow and survive. Only a tiny fraction of these survive. Yet so many are emitted from graupel, continuously during descent, that there is a significant effect overall.

(5) Homogeneously frozen cloud-droplets nucleate the vast majority of ice particles in the entire storm. Homogeneous freezing prevails in overall ice concentrations in the upper half of the mixed-phase region in stratiform regions of the storm.

(6) Multi-polarimetric radar properties, such as K_{DP}, are sensitive to inclusion of SIP in the simulation. Average K_{DP} in the upper half of the mixed-phase region is boosted by up to an order of magnitude from inclusion of breakup in ice-ice collisions in moderate to strong convective updrafts (> 4 m/s) and downdrafts (> 1 m/s), yet is reduced slightly in weaker ascent (< 4 m/s) and stratiform/cirriform cloud.

This last point (6) implies a new avenue of methodology: cloud models such as AC may be used to predict multi-polarimetric radar signatures of various ice multiplication mechanisms from correlations (e.g. K_{DP} in the phase-space of vertical velocity and temperature). Such signatures (e.g. **Fig. 6**) may then be sought in analysis of the corresponding radar observations in a wider variety of real storms.

Regarding points (3) and (4), tagging tracers are an innovative and powerful tool for analysis of the control simulation. They enable tracking of the various sources of ice particle number. By contrast, sensitivity tests are less useful for insight into the internal functioning of a given simulation in view of compensation by non-target processes.

In summary, the project has delineated the roles of four processes of SIP and primary ice production in various types of storm. This led to publications during the project describing new process-level representations and the role of SIP for storm electrification (Sec. 1.2.5). Codes for sublimational breakup and breakup during ice-ice collisions have been developed.

1.4. References for section I (the papers supported by this DOE grant are highlighted in blue)

Cantrell, W., and A. Heymsfield, 2005: Production of ice in tropospheric clouds: A review. *Bull. Am. Meteorol. Soc.*, **86**(6), 795-808

Deshmukh, A., Phillips, V. T. J., Bansemer, A., Patade, S., and D. Waman, 2022: New empirical formulation for the sublimational breakup of graupel and dendritic snow. *J. Atmos. Sci*., **79,** 317-336

Dong, Y., Oraltay, R. G., and J. Hallett, 1994: Ice particle generation during evaporation. *Atmos. Res.,* **32,** 45–53.

Field, P. R., and A. J. Heymsfield, 2015: Importance of snow to global precipitation. *Geophys. Res. Lett.*, **42**, 9512–9520

Field, P. R., Heymsfield, A. J., and A. Bansemer, 2006: Shattering and particle inter-arrival times measured by optical array probes in ice clouds. *J. Atmos. Sci*., **23,** 1357-1371

Field, P. R., Lawson, R. P., Brown, P., Lloyd, G., Westbrook, C., Moisseev, D., Miltenberger, A., Nenes, A., Blyth, A., Choularton, T., Connolly, P., Buehl, J., Crosier, J., Cui, Z., Dearden, C., DeMott, P., Flossmann, A., Heymsfield, A., Huang, Y., Kalesse, H., Kanji, Z., Korolev, A.,

Kirchgaessner, A., Lasher-Trapp, S., Leisner, T., McFarquhar, G., Phillips, V., Stith, J., and S. Sullivan, 2017: Chapter 7. Secondary Ice Production - current state of the science and recommendations for the future. In "*Ice Formation and Evolution in Clouds and Precipitation: Measurement and Modeling Challenges*", Meteorological Monographs, No. 58 (Chapter 7)**,** 7.1-7.19.

Fletcher, N. H., 1962*: The Physics of Rainclouds,* 386 pp., Cambridge Univ. Press, New York.

Fridlind, A. M., Li, X., Wu, D., van Lier-Walqui, M., Ackerman, A. S., Tao, W., McFarquhar, G. M., Wu, W., Dong, X., Wang, J., Ryzhkov, A., Zhang, P., Poellot, M. R., Neumann, A., and J. M. Tomlinson, 2017: Derivation of aerosol profiles for MC3E convection studies and use in simulations of the 20 May squall line case. *Atmos. Chem. Phys.*, **17**(9), 5947-5972.

Hallett, J., and S. C. Mossop, 1974: Production of secondary ice particles during the riming process. *Nature*, **249**, 26–28

Hobbs, P. V., Politovich, M. K. and Radke, L. F., 1980: The structures of summer convective clouds in eastern Montana. I: Natural clouds. *J. Appl. Meteor.,* **19,** 645–663

Huang, Y., Wu, W., McFarquhar, G. M., Xue, M., Morrison, H., Milbrandt, J., Korolev, A. V., Hu, Y., Qu, Z., Wolde, M., Nguyen, C., Schwarzenboeck, A., and Heckman, I.: Microphysical processes producing high ice water contents (HIWCs) in tropical convective clouds during the HAIC-HIWC field campaign: dominant role of secondary ice production. *Atmos. Chem. Phys*., **22**, 2365–2384

Johnson, D. A., and J. Hallett, 1968: Freezing and shattering of supercooled water drops. *Quart. J. Roy. Meteor. Soc*., **94**, 468–482

Korolev, A. V., Emery, E. F., Strapp, J. W., Cober, S. G., Isaac, G. A., Wasey, M., and D. Marcotte, 2011: Small ice particles in tropospheric clouds: fact or artifact? Airborne icing instrumentation evaluation experiment. *Bull. Amer. Meteor. Soc*., **92,** 967–973

Lasher-Trapp, S., D. C. Leon, P. J. DeMott, C. M. Villanueva-Birriel, A. V. Johnson, D. H. Moser, C. S. Tully, and W. Wu, 2016: A multisensor investigation of rime splintering in tropical maritime cumuli. *J. Atmos. Sci*., **73**, 2547–2564

Lasher-Trapp, S., Scott, E.L., Järvinen, E., Schnaiter, M., Waitz, F., DeMott, P.J., McCluskey, C.S. and Hill, T.C., 2021: Observations and modeling of rime splintering in Southern Ocean cumuli. *J. Geophys. Res: Atmospheres*, **126**(23), e2021JD035479

Lawson, R. P., S. Woods, and H. Morrison, 2015: The microphysics of ice and precipitation development in tropical cumulus clouds. *J. Atmos. Sci*., **72**, 2429–2445

Lohmann, U., and J. Feichter, 2005: Global indirect aerosol effects: a review. *Atmospheric Chemistry and Physics,* **5**(3), 715-737

Matus, A. V., and T. S. Ecuyer, 2017: The role of cloud phase in Earth's radiation budget. *J. Geophys. Res*., **122**, 2559-2578

Oraltay, R. G., and J. Hallett. 1989: Evaporation and melting of ice crystals: A laboratory study. *Atmos. Res*., **24,** 169–189

Patade, S., V. T. J., Phillips, P., Amato, H. G., Bingemer, S. M., Burrows, P. J., DeMott, P. J., Goncalves, F. L. T., Knopf, D. A. Morris, C. E., Alwmark, C., Artaxo, P., Pöhlker, C., Schrod,

J., and B. Weber, 2021: Empirical formulation for multiple groups of primary biological ice nucleating particles from field observations over Amazonia. *J. Atmos. Sci.*, **78** (7), 2195-2220.

Patade, S., V. T. J. Phillips, D. Waman, A. Deshmukh, A. K. Gupta, A. Jadav, A. Bansemer, J. Carlin, and A. Ryzhkov, 2022: The influence of multiple groups of biological ice nucleating particles on microphysical properties of mixed-phase clouds observed during MC3E. *Atmos. Chem. Phys*., **22**, 12055-12075

Phillips, V. T. J., Andronache, C., Christner, B., Morris, C.E., Sands, D.C., Bansemer, A., Lauer, A., McNaughton, C. and C. Seman, 2009. Potential impacts from biological aerosols on ensembles of continental clouds simulated numerically. *Biogeosciences*, **6,** 1–28

Phillips, V.T. J., Demott, P.J., Andronache, C., Pratt, K.A., Prather, K.A., Subramanian, R., and C. Twohy, 2013. Improvements to an empirical parameterization of heterogeneous ice nucleation and its comparison with observations. *J. Atmos. Sci.*, **70**(2), 378-409

Phillips, V. T. J., Khain, A., Benmoshe, N., and E. Ilotoviz, 2014: Theory of time-dependent freezing and its application in a cloud model with spectral bin microphysics. I: Wet growth of hail. *J. Atmos. Sci*, **71,** 4527–4557

Phillips, V. T. J., Khain, A., Benmoshe, N., Ilotoviz, E., and A. Ryzhkov, 2015a: Theory of time-dependent freezing and its application in a cloud model with spectral bin microphysics. II: Freezing raindrops and simulations. *J. Atmos. Sci.*, **72,** 262–286

Phillips, V. T. J., Formenton, M., Bansemer, A., Kudzotsa, I., and B. Lienert, 2015b: A parameterization of sticking efficiency for collisions of snow and graupel with ice crystals: theory and comparison with observations. *J. Atmos. Sci*., **72,** 4885–4902

Phillips, V. T. J., J. I., Yano, A., Khain, 2017: Ice multiplication by breakup in ice-ice collisions. Part I: Theoretical formulation, *J. Atmos. Sci.*, **74**(6), 1705–1719

Phillips, V. T. J., J. I., Yano, M., Formenton, E., Ilotoviz, V. P., Kanawade, I., Kudzotsa, J., Sun, A., Bansemer, A. G., Detwiler, A., Khain, S. A., Tessendorf, 2017: Ice multiplication by breakup in ice-ice collisions. Part II: Numerical simulations, *J. Atmos. Sci.*, **74**(9), 2789–2811

Phillips, V. T. J., S. Patade, J., Gutierrez, A., Bansemer, 2018: Secondary ice production by fragmentation of freezing drops: Formulation and theory, *J. Atmos. Sci.*, **75**(9), 3031–3070

Phillips, V. T. J., M., Formenton, V. P., Kanawade, L. R., Karlsson, S. Patade, J., Sun, C., Barthe, J. P., Pinty, A. G., Detwiler, W., Lyu, S. A., Tessendorf, 2020: Multiple environmental influences on the lightning of cold-based continental cumulonimbus clouds. Part I: Description and validation of model, *J. Atmos. Sci.*, **77**(12), 3999–4024

Phillips, V. T. J., and S. Patade, 2022: Multiple environmental influences on the lightning of cold-based continental cumulonimbus clouds. Part II: sensitivity tests for its charge structure and land-ocean contrast. *J. Atmos. Sci.*, **79,** 263–300

Pruppacher, H. and J. Klett, 1997: *Microphysics of clouds and precipitation*. Kluwer Academic Publishers.

Rosenfeld, D. and W. L Woodley, 2000: Deep convective clouds with sustained supercooled liquid water down to −37.5 ◦C. *Nature*, **405**, 440–442

Solomon, S., Qin, D., Manning, M., Chen, Z., Marquis, M., Averyt, K., Tignor, M., and H. L. Miller (eds.), 2007: *Climate change 2007: The physical science basis. Contribution of Working Group I to the fourth assessment report of the intergovernmental panel on climate change, (IPCC).* Cambridge University Press, Cambridge, United Kingdom and New York, NY, USA

Takahashi, C., and A. Yamashita, 1977: Production of ice splinters by the freezing of water drops in free fall. *J. Meteor. Soc. Japan*, **55**, 139–141

Takahashi, T., Nagao, Y. and Y. Kushiyama, 1995: Possible high ice particle production during graupel-graupel collisions. *J. Atmos. Sci.*, **52,** 4523-4527

Vardiman, L., 1978: The generation of secondary ice particles in clouds by crystal-crystal collision. *J. Atmos. Sci*., **35,** 2168-2180

Waman, D., A. Jadav, A. Deshmukh, V. T. J. Phillips, S. Patade, A. K. Gupta, A. Bansemer, 2022: Dependencies of four mechanisms of secondary ice production on cloud top temperature in a continental convective storm. *J. Atmos. Sci.*, **79,** in press

Zhao, X., X. Liu, V. T. J. Phillips, and S. Patade, 2021: Impacts of secondary ice production on Arctic mixed-phase clouds based on ARM observations and CAM6 single-column model simulations. *Atmos. Chem. Phys.,* **21**, 5685–5703

II. Modeling studies at the Hebrew University of Jerusalem

2.1. The development of novel bin-microphysics 3D model for calculation of polarimetric signature from mesoscale phenomena. Implementation of detailed melting

A new Fast Spectral Bin Microphysics scheme (FSBM-2) that was developed and embedded into the Weather Research and Forecasting Model (WRF). FSBM-2 was used to simulate a mesoscale deep convective system observed during the Midlatitude Continental Convective Clouds Experiment (MC3E). The model was able to simulate a realistic geometrical structure and main microphysical parameters of the mesoscale convective system observed on 20 May 2011 including radar reflectivity and precipitation rate. Moreover, the FSBM-2 was able to reproduce rain size distributions at different rain rates measured using surface sensors. To illustrate this result, we present Fig. 2.1 that compares stratiform surface rain mass distribution retrieved from the model and measured by the Parsivel disdrometer – PD (gray circles) at different precipitation rates. The results of three simulation versions are shown: H43, where all size distributions were defined using a mass grid containing 43 mass bins and the high-density hydrometeor had properties of hail (density, fall velocity, etc.); H33 is similar to H43, but only 33 mass bins were used (i.e. maximum size of hail was about 0.9 cm); and G33, in which high density particles had properties of graupel. This version of FSBM-2 is included into the new release of the WRF Version 4.2.

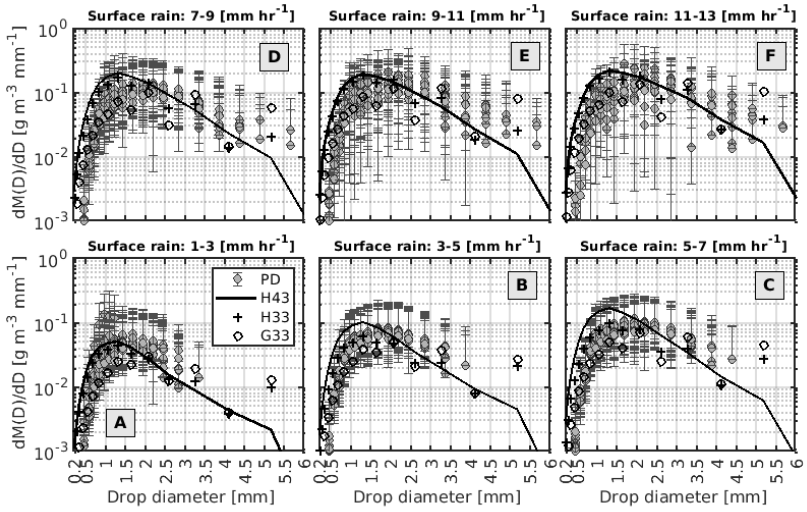

Fig. 2.1. *Stratiform surface rain mass distribution in observations (Parsival distrometer - PD, gray circles) and in simulations (black line – H43, black plus – H33 and black diamond – G33). For the observation, 16 PDs were used, giving rain rate and rain size distribution over 32-diameter size bins within the interval 0.06–25.2 mm. Gray circles represent the mean value in each size bin in each distrometer for the corresponding rain rate between 11-13 UTC. The bars correspond to 10th and 90th percentiles. For the simulation, the mean value is presented within the stratiform area defined by the rectangle in the northern part of the squall line at 9:00-10:00 UTC of the simulation with 10 min output frequency.*

Initial version of FSBM-2 includes a simplified melting procedure, according to which each hydrometeor has its own melting rate, so that the mass of ice decreases, and the corresponding mass is added to mass of raindrops. No particles contained both ice and water (i.e. particles with liquid water fraction) are considered. As a result, the simplified approach to melting used in the first version of FSBM-2 does not allow to reproduce realistic polarimetric radar signatures below the melting level. In particular, no bright bands in terms of radar reflectivity Z and differential reflectivity Z_{DR} were reproduced.

Taking into account high importance of the microphysical and dynamical processes in the boundary layer, which can be observed and interpreted using the polarimetric radar signatures, a procedure of detailed melting was implemented into FSBM-2 (Shpund et al, 2022, in preparation). The procedure of melting is described in detail in Khain and Pinsky (2018). The procedure has been implemented into HUCM and used in the studies by Ryzhkov et al. (2011) and Ilotoviz et al. (2014, 2016, 2018). A detailed melting procedure calculates the liquid water content (or liquid water fraction LWF) in melting particles. If LWF in melting particles increases up to 0.99, the ice particle is assumed to be completely melt. The procedure implemented in FSBM-2 allows for collisions of melting particles with all other hydrometeors and between melting particles themselves.

Fig. 2.2 shows vertical distribution (CFAD) of radar reflectivity in H43 using a simple melting procedure (left) and detailed melting (center). One can see a good agreement with observations (right panel). A bright band is clearly seen. Besides, detailed melting leads to formation of larger raindrops (larger Z).

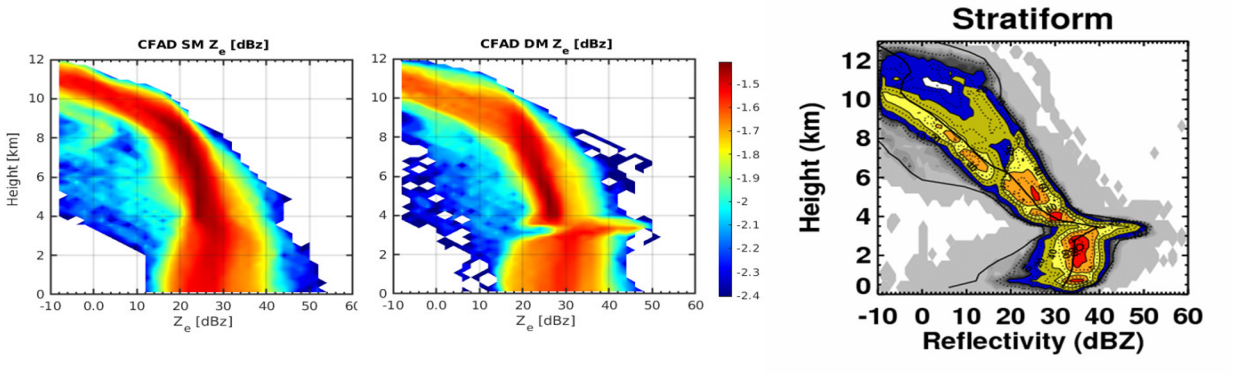

Fig. 2.2. *Vertical distribution (CFAD) of radar reflectivity in stratiform area in H43 calculated using a simple melting procedure (left) and detailed melting (center). One can see a good agreement with observations (right panel).*

2.7 Development of the theory of ice multiplication by drop freezing

One of the mysteries in the cloud microphysics is the fact that the concentration of ice crystals in clouds is higher than the concentration of ice nuclei (IN) (which nucleation leads to formation of ice crystals) by several orders of magnitude. For instance, concentration of IN in the ICE-T field experiment was evaluated varying from $10^{-4}\ L^{-1}$ at $T = -5\,^{o}C$ to $10^{-1}\ L^{-1}$ at $-20\,^{o}C$ (Lasher-Trapp et al. 2016), while the measured ice crystal concentration in the clouds was of several hundred per liter. It is a general consensus that ice crystals form by the mechanisms of secondary ice formation.

The mechanisms of the drop splintering are not well known. In our study (Staroselsky et al. 2021) a detailed process of droplet freezing is simulated. It is assumed that splintering and droplet fragmentation during droplet freezing takes place because of dendritic growth within a supercooled drop. The process of dendritic growth during the freezing process simulated by a new model able to capture the process of solidification is illustrated in Fig. 2.3. Figure 2.3 shows the transient evolution of solid fraction as the solidification progresses from the center of a droplet with diameter 0.3 mm. Due to a hexahedral symmetry of a solid water crystal, 6 primary trunks initially grows from a single seed laced at the center of a droplet. However, at t = 0.015 s prominent secondary and tertiary arms start growing and the dendrite arm eventually reaches the surface of the droplet. Once the growth from surface starts to dominate the dendritic growth, some small closed volume of liquid water can be observed (t=0.09 s). This becomes more prominent as time evolves (t=0.15s) and eventually may lead to fracture. The droplet takes around 0.3 s to completely solidify.

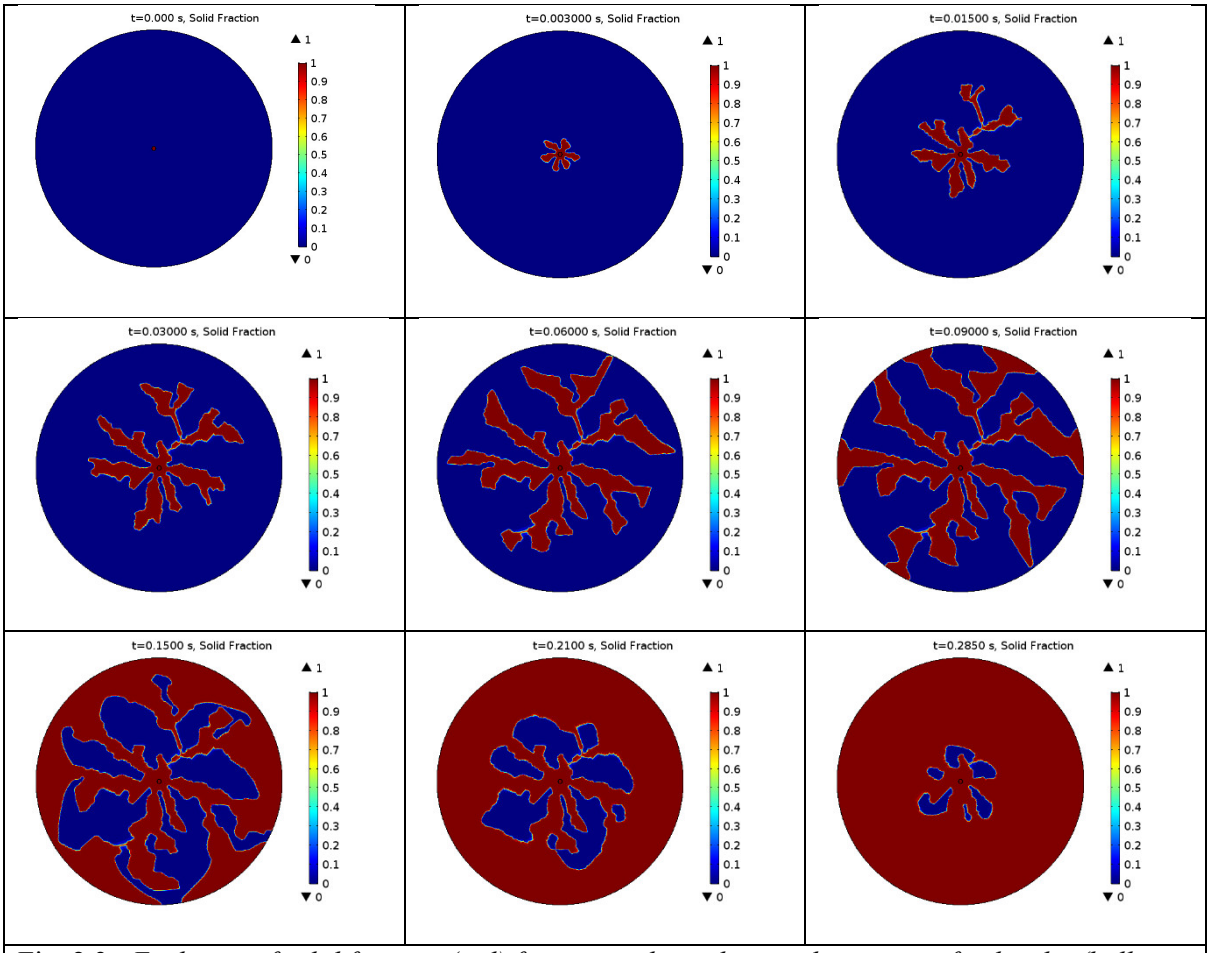

Fig. 2.3. *Evolution of solid fraction (red) from a single nucleus at the center of a droplet (bulk nucleation)*

As soon as the closed water volumes arise within the freezing drop, further freezing leads to formation of internal stresses. Numerical modeling of the drop freezing process shows that the maximum number of filaments and liquid volumes take place within the temperature range -10°C to -15°C, which agrees with laboratory results. At warmer temperatures, dendritic growth is inefficient. At very low (cold) temperatures, the freezing process takes place like a planar front. In both cases, the intensity of splintering decreases or dendrites do not grow at all. In this case no internal stresses arise within a freezing drop and no splintering takes place. We showed that number of splinters is close to that of the isolated volumes filled by water and forming during dendrite growth.

2.3. Implementation of SIP in the LES

Usually three SIP mechanisms are discussed in the literature (Phillips et al. 2018, Phillips et al. 2017a, Phillips et al. 2017b, Khain and Pinsky 2018). All of them are found under laboratory conditions. The first one is a well-known Hallett-Mossop (HM) mechanism, according to which collisions of drops (with radii exceeding 24 μm) and graupel at temperatures within the range −3 ^{o}C to −8 ^{o}C lead to formation of ice splinters, with one splinter per about 250 collisions (Hallett and Mossop 1974). This mechanism in a parameterized form is included into the most cloud resolving models (CRM) with explicit microphysics.

The second ice splintering mechanism is related to the production of ice fragments during drop freezing (mode 1) and during drop-ice collisions (mode 2) that is accompanied by freezing of liquid at the surface of ice particles.

In the course of this project, a modified version of HUCM was developed which includes parameterization of ice multiplication. The semi-empiric parameterizations based on the results of laboratory measurements are developed by Phillips et al. (2017b, 2018). In contrast to a parcel model used by Phillips et al., we use the 2D mixed-phase HUCM with spectral bin microphysics which allows us to take into account several microphysical processes, including entrainment and mixing of clouds with environment, variability of vertical velocities and other microphysical parameters as well as precipitation formation. HUCM simulates the entire cloud evolution of a mixed-phase cloud, which allows us to simulate and analyze all the three ice multiplication mechanisms mentioned above and determine the comparative role of each mechanism at different stages of cloud evolution.

One of the important goals of this study was to analyze the role of aerosol concentration and shapes of aerosol size distributions on the process of ice multiplication. In a set of simulations with HUCM, it was shown that both splintering mechanisms can produce ice particle concentrations of several hundred per liter. Ice formation starts from primary nucleation and drop freezing. Then ice multiplication mechanism related to drop freezing and drop-ice collisions becomes very efficient leading to cloud glaciation. Glaciation leads to weakening of the ice production mechanism related to drops. At the same time, formation of secondary ice by ice-ice collisions remains efficient during all cloud life cycle.

The results of simulations agree well with the in-situ measurements in growing convective cloud (Lawson et al. 2015). Effects of the aerosol concentration on concentration of ice crystals are illustrated in Fig 2.4. One can see that there is the CCN concentration N_o =1000 cm^{-3} that leads to the maximum secondary ice production. At such significant concentrations, many raindrops freeze producing ice splinters. At lower CCN concentrations many raindrops fall down without freezing.

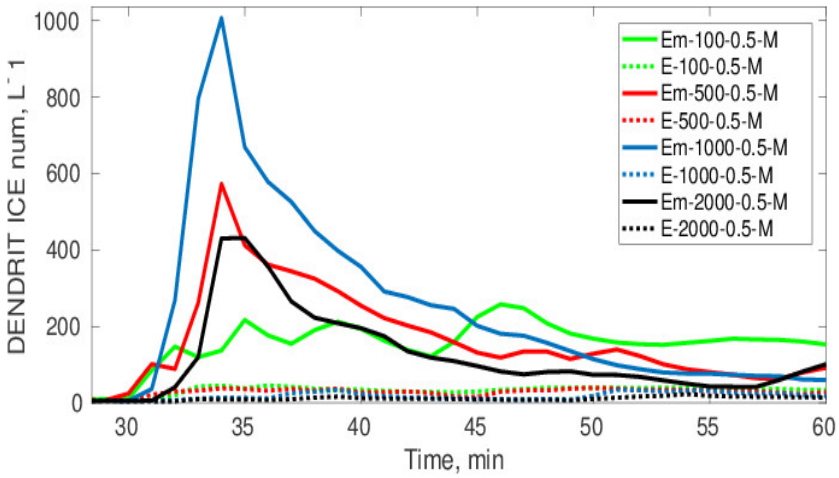

Fig. 2.4. *Time dependences of maximum number concentration of ice crystals (dendrites) forming by drop freezing and drop-ice collisions in simulations with different No and k = 0.5 (solid lines) (the parameters in the Twomey formula Nccn= $N_{ccn} = N_o S^k$, where S is the supersaturation with respect to water. For comparison, time dependences of the maximum dendrite number concentrations in simulations without raindrop-freezing fragmentation (mode 1 and mode 2) processes are presented as well (dashed lines). The measurements in Lawson et al. (2015) show that the ice number concentration is up to 500 L^{-1}.*

2.4. Investigation of the processes of mixing of clouds and environment and their effects on cloud structure

Several studies were performed to investigate the role of entrainment and mixing on cloud microphysics and cloud geometry (Pinsky and Khain, 2018; 2019a,b). It was shown that effect of mixing is substantial for small clouds and low vertical velocities. Large clouds have cloud cores which are close to undiluted. It was shown that clouds are surrounded by humid shell with enhanced humidity. At the decaying stage, clouds evaporate largely due to air sedimentation (adiabatic heating), but its horizontal sizes are strongly affected by intensity of mixing.

Recently, we initiated a new direction in the investigation of cloud processes. Motion in clouds have a wide range of scales, from 1 cm to the scales of a cloud. The roles of the motions of different scales are different. Convective scales (coherent scales) form a cloud skeleton. These motions transport mass and determine mass fluxes, entrainment and detrainment in clouds. At the same time, turbulent motions lead to smoothing the gradients and affect cloud microphysics largely near cloud edges. Note that turbulent motions do not transport mass and they are stochastic. We have developed a method of scale separation to investigate the roles of the motions of different scales using wavelet techniques and evaluated properties of both convective and turbulent motions and their effect on a cloud structure. It was found that entrainment is caused by toroidal vortices

forming at the upper part of developing clouds. These vortices cause deep convective scale penetration of environment air to clouds (Eytan et al. 2021, 2022; Pinsky et al, 2022).

2.5. Future studies

Future theoretical studies aim at improvement of FSBM-2 by implementation of detailed melting procedure as well as by implementation of ice multiplication mechanisms. The new version of FSBM-2 will be used for simulation of storms and tropical cyclones. Since bin-microphysics models contain a large number of variables (several hundred) (because each bin in size distributions represent a separate field), the bin microphysics schemes are time consuming. Advection of such high number of variables (especially in 3D) requires significant CPU time. Significant efforts have been made recently to develop an efficient advection scheme. First tests of the new advection scheme showed that the new scheme requires 5 - 10 times less CPU time than the standard schemes applied in WRF. Testing and further improvement of the advection scheme will be continued during our future studies.

We will continue working with the LES cloud model with resolution of 10 m with the aim of development of accurate parameterization of cloud-environment interaction in the ice phase and investigation of ice formation.

2.6 References for section II (the papers supported by this DOE grant are highlighted in blue)

Eytan, E., Koren, I., Altaratz, O., Pinsky, M., and Khain, A.: Revisiting adiabatic fraction estimations in cumulus clouds: high-resolution simulations with a passive tracer, *Atmos. Chem. Phys*., **21**, 16203–16217, https://doi.org/10.5194/acp-21-16203-2021, 2021.

Eytan, E., A. Khain, M. Pinsky,O. Altaratz, J.Shpund, and I. Koren, 2022: Shallow Cumulus Properties as Captured by Adiabatic Fraction in High-Resolution LES Simulations. *J. Atmos. Sci*.**79**, 409–428; doi:10.1175/JAS-D-21-0201.1.

Fan J., D. Rosenfeld, Y. Zhang, S. E Giangrande, Z. Li, Luiz AT Machado, S. T Martin, Y. Yang, J. Wang, P. Artaxo, H. MJ Barbosa, R. C Braga, J. M Comstock, Z. Feng, W. Gao, H. B Gomes, F. Mei, C. Pöhlker, M. L Pöhlker, U. Pöschl, R. AF de Souza, 2018: Substantial convection and precipitation enhancements by ultrafine aerosol particles. *Science* 359 (6374), 411-418.

Fridlind, A., A. Ackerman, A. Grandin, F. Dezitter, M. Weber, J. Strapp, A. Korolev, and C. Williams, 2015: High ice water content at low radar reflectivity near deep convection – Part 1: Consistency of in situ and remote-sensing observations with stratiform rain column simulations. *Atmos. Chem. Phys*., **15**, 11713 – 11728.

Fridlind A. M., X. Li, D. Wu, M. van Lier-Walqui, A. S. Ackerman, W.-K. Tao,G. M. McFarquhar, W. Wu, Xiquan Dong, J.Wang, A. Ryzhkov, P. Zhang,M. R. Poellot, A. Neumann, and J. M. Tomlinson, 2017: Derivation of aerosol profiles for MC3E convection studies and usein simulations of the 20 May squall line case, *Atmos. Chem. Phys.*, 17, 5947–5972; www.atmos-chem-phys.net/17/5947/2017/doi:10.5194/acp-17-5947-2017.

Hallett, J., and S. Mossop (1974), Production of secondary ice particles during the riming process, *Nature*, **249** (5452), 26.

Heymsfield A. J., A. Bansemer, G. Heymsfield, and A.O. Fierro, 2009: Microphysics of maritime tropical convective updrafts at temperatures from -20° *C* to -60° C, *J. Atmos. Sci.,* **66**, 3530-3565.

Hu, J., A. Ryzhkov, D. Rosenfeld, P. Zhang, 2020: Synergetic use of the WSR-88D radars, GOES-R satellites, and lightning sensors to study microphysical characteristics of hurricanes. *J. Appl. Meteor. Clim*., **59**, 1051 – 1068.

Hu, J., D. Rosenfeld, A. Ryzhkov, D. Zrnic, E. Williams, P. Zhang, J. Snyder, R. Zhang, and R. Weitz, 2019: Polarimetric radar convective cell tracking reveals large sensitivity of cloud precipitation and electrification properties to CCN. *J. Geophys. Res.. Atmosphere,* **124**, 12194 – 12205.

Khain, A. P., V. Phillips, N. Benmoshe, and A. Pokrovsky, 2012: The role of small soluble aerosols in the microphysics of deep maritime clouds, *Journal of the Atmospheric Sciences*, **69** (9), 2787–2807.

Khain, A. P., and M. Pinsky, 2018: *Physical Processes in Clouds and Cloud Modeling*, Cambridge University Press., 642 pp.

Lang, T. J., L. J. Miller, M. Weisman, S. A. Rutledge, L. J. Barker III, V. Bringi, V. Chandrasekar, A. Detwiler, N. Doesken, J. Helsdon, et al. (2004), The severe thunderstorm electrification and precipitation study, *Bull. Amer. Meteorol. Soc.,* **85** (8), 1107–1126.

Lasher-Trapp, S., D. C. Leon, P. J. DeMott, C. M. Villanueva-Birriel, A. V. Johnson, D. H. Moser, C. S. Tully, and W. Wu (2016), A multisensor investigation of rime splintering in tropical maritime cumuli. *J. Atmos. Sci.*, **73** (6), 2547– 2564.

Lawson, R. P., S. Woods, and H. Morrison, 2015: The microphysics of ice and precipitation development in tropical cumulus clouds, *J. Atmos. Sci.,* **72** (6), 2429–2445.

Leroy, D., E. Fontane, A. Schwarzenboeck, J. Strapp, A. Korolev, G. McFarquhar, R. Dupuy, C. Courbeyre, L. Lilie, A. Protat, J. Delanoe, F. Dezitter, and A. Grandin, 2017: Ice crystal sizes in high ice water content clouds. Part II: Statistics of mass diameter percentiles in tropical convection observed during the HAIC/HIWC project. *J. Atmos. Oceanic Technol.*, **34**, 117 – 136.

Meyers, M. P., P. J. DeMott, and W. R. Cotton, 1992: New primary ice-nucleation parameterizations in an explicit cloud model. *J. Appl. Meteorol.*, **31** (7), 708–721.

Phillips, V. T., J.-I. Yano, and A. Khain, 2017: Ice multiplication by breakup in ice–ice collisions. part i: Theoretical formulation. *J. Atmos. Sci.*, **74** (6), 1705–1719.

Phillips, V. T., J.-I. Yano, M. Formenton, E. Ilotoviz, V. Kanawade, I. Kudzotsa, J. Sun, A. Bansemer, A. G. Detwiler, A. Khain, et al., 2017b: Ice multiplication by breakup in ice–ice collisions. part ii: Numerical simulations. *J. Atmos. Sci.*, **74** (9), 2789–2811.

Phillips, V. T., S. Patade, J. Gutierrez, and A. Bansemer, 2018: Secondary ice production by fragmentation of freezing drops: Formulation and theory. *J. Atmos. Sci.*, **75** (9), 3031–3070.

Pinsky, M., and A.P. Khain, 2018: Theoretical Analysis of the Entrainment–Mixing Process at Cloud Boundaries. Part I: Droplet Size Distributions and Humidity within the Interface Zone. *J. Atmos. Sci*., **75** (6), 2049-2064.

Pinsky, M., and A.P. Khain, 2019: Theoretical analysis of entrainment-mixing at cloud boundaries. Part II: motion of cloud interface, *J. Atmos. Sci*. **76**, 2599 – 2616.

Pinsky M., and A. Khain, 2020: Analytical investigation of the role of lateral mixing in the evolution of non-precipitating Cu. Part 2: Dissolving stage *J. Atmos. Sci.* **77**, 911 – 924.

Pinsky M., E. Eytan, I. Koren, and A. Khain, 2022: Convective and turbulent motions in non-precipitating Cu. Part II: LES simulated cloud represented by a starting plume. *J. Atmos. Sci.*, **79**, 793-813, DOI: 10.1175/JAS-D-21-0137.1

Ryzhkov, A., Pinsky, M., Pokrovsky, A., & Khain, A. (2011). Polarimetric radar observation operator for a cloud model with spectral microphysics. *J. Appl. Meteorol Climatol.* **50** (4), 873–894.

Ryzhkov, A., and D. Zrnic, 2019: *Radar Polarimetry for Weather Observations*. Springer, 486 pp.

Rosenfeld, D., W.L. Woodley (2000), Deep convective clouds with sustained highly supercooled liquid water until - 37.5°C, *Nature,* **405**, 440-442.

Shpund J., A. Khain, B. Lynn, J. Fan, B. Han, A. Ryzhkov, J. Snyder, J. Dudhia, D. Gill, 2019: Simulating a Mesoscale Convective System Using WRF with a New Spectral Bin Microphysics - Part 1: Hail vs Graupel. *J. Geophys. Res*., **124**, 14072 – 14101.

Strapp, J. W., and Coauthors, 2016: *The High Ice Water Content* (HIWC) *study of deep convective clouds*: *Report on science and technical plan*. FAA Rep. DOT/FAA/TC-14/31, 105 pp. [Available online at www.tc.faa.gov/its/worldpac/techrpt/tc14-31.pdf.

Staroselsky A., R. Acharya, A. Khain, 2021: Toward the theory of droplet fragmentation by freezing. *J. Atmos. Sci*., **78**, 3181–3204, https://doi.org/10.1175/JAS-D-20-0029.1

III. Observational studies at the University of Oklahoma. Polarimetric radar microphysical retrievals in ice, their validation, and climatology.

3.1 Polarimetric radar microphysical retrievals in ice

In addition to the radar reflectivity factor Z, modern polarimetric weather radars (research and operational) measure differential reflectivity Z_{DR}, differential phase Φ_{DP}, and cross-correlation coefficient ρ_{hv} between horizontally and vertically polarized radar returns. A very important polarimetric variable, specific differential phase K_{DP} is estimated from a radial profile of Φ_{DP} as a half of the radial derivative of Φ_{DP}. Polarimetric radar measurements can be efficiently utilized for retrievals of key microphysical variables, such as precipitation fluxes, liquid water content (LWC) or ice water content (IWC), particle characteristic sizes such as the mean volume diameter D_m, and their total number concentration N_t. We have recently developed a number of various polarimetric retrieval relations in ice involving Z, Z_{DR}, and K_{DP} which can be found in Ryzhkov and Zrnic (2019, Chapter 11), Ryzhkov et al. (2020), Bukovcic et al. (2018, 2020), Carlin et al. (2021), and Dunnavan et al. (2022). These relations are primarily applicable in the stratiform parts of the storms in the absence of large graupel and hail.

The most useful polarimetric radar variable for ice retrievals is K_{DP} which is proportional to the first moment of the ice particle size distributions (PSD) and is better correlated with IWC than Z that is proportional to the 4th moment of PSD in ice and snow. The big advantage of K_{DP} is that it is not biased by noise, attenuation, and radar miscalibration. On the other hand, the magnitude of K_{DP} in ice and snow is relatively small, particularly at longer radar wavelengths. This dictates the need to do spatial averaging of K_{DP} to reduce a statistical error of the K_{DP} estimation. Novel techniques for radar data processing and visualization have been introduced to perform such averaging. These include the quasi-vertical profile (QVP) methodology (Ryzhkov et al. 2016), as well as the range-defined QVP (RD-QVP) (Tobin and Kumjian 2017) and columnar vertical profiles (CVP) (Murphy et al. 2020) techniques. The QVP and RD-QVP products represent vertical profiles of radar variables and microphysical parameters averaged over the area centered on the radar location with a typical diameter of 100 km. As opposed to QVP and RD-QVP, the CVP product is not radar-centric and the corresponding vertical column can be placed anywhere within the radar coverage area. A typical horizontal size of such a column is 20 km x 20°. The quasi-vertical and columnar vertical profiles are commonly represented in a height vs time format which allows to capture the vertical structure of the storm and its temporal evolution with unprecedented resolution.

An example of CVPs for hurricanes Harvey and Florence observed with the KCPR and KLTX WSR-88D radars is shown in Fig. 3.1. The CVPs have been generated for the vertical column with the horizontal size of 20 km x 20° moving along the major hurricane track. Such representation of the radar data reveals strong vertical gradients of Z, K_{DP}, Z_{DR}, and corresponding rain rate below the melting layer which are typical for "warm" rain process. The vertical profiles of such microphysical variables as liquid and ice water content (LWC / IWC), mean volume diameter D_m and total number concentration N_t of hydrometeors can be retrieved from the vertical profiles of radar variables (Fig. 3.2).

Similar analysis of the QVP and CVP profiles of radar variables and microphysical parameters has been performed for a number of archetypal continental and tropical storms observed with the operational WSR-88D radars in the US and with the research polarimetric radars in different parts of the world. The latter ones include the NCAR S-Pol radar that observed tropical clouds in the middle of Indian Ocean during the DYNAMO field campaign and the C-Pol radar in Darwin, Australia. Numerous examples of the corresponding QVPs and CVPs are shown in the two previous annual reports for this project.

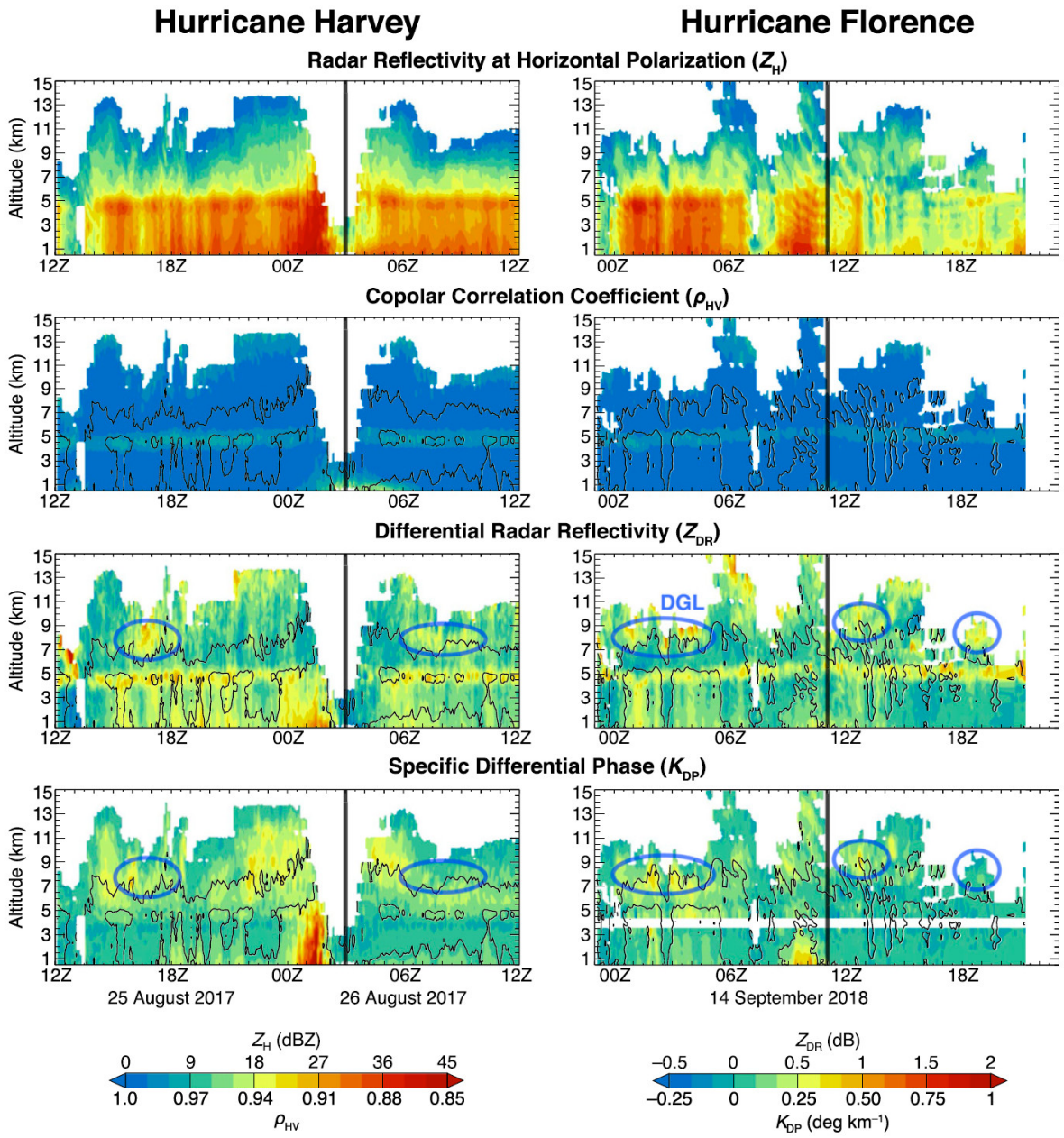

Fig. 3.1. *Columnar vertical profiles (CVPs) of Z, Z_{DR}, K_{DP}, and cross-correlation coefficient ρ_{hv} for hurricanes Harvey and Florence. CVPs along the hurricanes' tracks were created using data from the Corpus Christi, TX, radar (KCRP) for hurricane Harvey, and from the Wilmington, NC, radar (KLTX) for hurricane Florence. From Homeyer et al. (2021).*

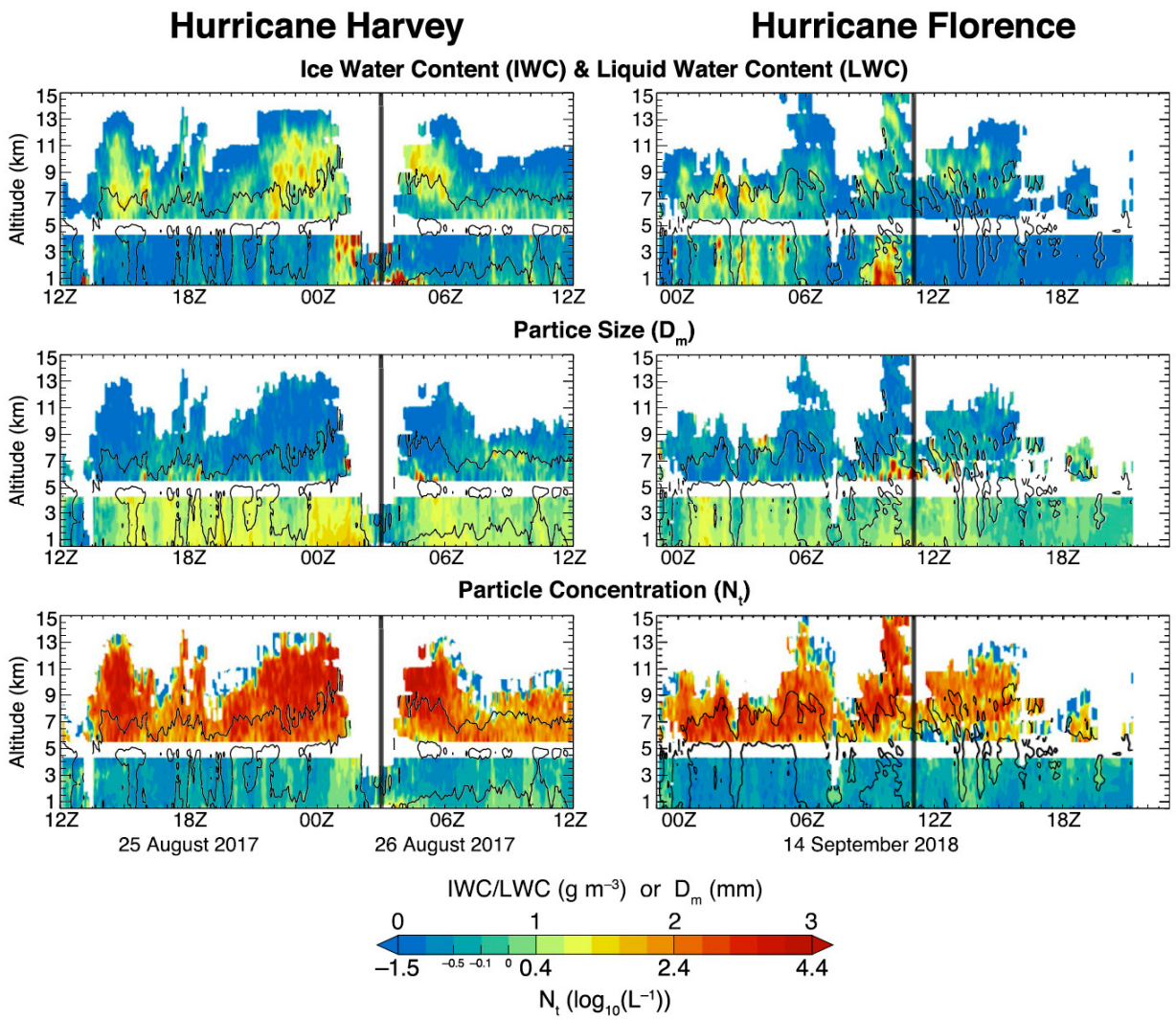

Fig. 3.2. *CVPs of liquid / ice water content (LWC / IWC), mean volume diameter (D_m), and total number concentration (N_t) of hydrometeors for hurricanes Harvey and Florence retrieved from the polarimetric radar data shown in Fig. 5. From Homeyer et al. (2021).*

3.2 Validation of the polarimetric microphysical retrievals in ice

Validation of our methodologies for polarimetric microphysical retrievals in ice requires comparisons with in situ microphysical measurements onboard research aircrafts. Therefore, we used every opportunity to look at the aircraft microphysical data collected in the proximity of ground-based polarimetric radars or combined with the data from polarimetric radars onboard the same aircraft. Such opportunities were offered during multiple field campaigns. A list of these campaigns, research aircrafts, and polarimetric radars involved is in Table 3.1.

Table 3.1. *List of field campaigns used for validation of the radar microphysical retrievals in ice.*

	Name of campaign	Year	Aircraft	Radar
1	Midlatitude Continental Convective Clouds Experiment (MC3E), USA	2011	UND Cessna Citation II	WSR-88D
2	Plains Elevated Convection At Night (PECAN), USA	2015	NOAA P3	WSR-88D
3	High Altitude Ice Crystals – High Ice Water Content (HAIC – HIWC), French Guiana	2015	Canada NRC Convair 580	Aircraft X-band radar
4	Olympic Mountains Experiment (OLYMPEX), USA	2015 - 2016	UND Cessna Citation II	Doppler on Wheels X-band radar
5	In-Cloud Icing and Large-drop Experiment (ICICLE), USA	2019	Canada NRC Convair 580	Aircraft X-band radar
6	Investigations of Microphysics and Precipitation for Atlantic Coast-Threatening Snowstorms (IMPACTS), USA	2020	NOAA P3	WSR-88D

One of the great challenges in validating the results of the radar microphysical retrievals using aircraft in situ probes is the problem of spatial / temporal matching of the radar and aircraft data which have very different sampling volumes and are obtained at different update times. The best results have been obtained using collocated radar and microphysical sensors onboard the same aircraft. This was possible with the Canadian National Research Council (NRC) Convair 580 aircraft that carries both in situ microphysical probes and the X-band polarimetric radar (Nguyen et al. 2019). Nguyen et al. (2019) tested our polarimetric radar retrieval algorithm for estimation of ice water content (IWC) for several Convair 580 fights within tropical storms during the HAIC – HIWC experiment in Cayenne, French Guiana. It was shown that the IWC(K_{DP}, Z_{DR}) relation suggested by Ryzhkov et al. (1998) provides very accurate estimate of IWC as opposed to the conventional IWC(Z) relation by Hogan et al. (2006). Similar aircraft observations during the ICICLE field campaign in the US Midwest demonstrate the ability of the polarimetric airborne radar to determine the mean volume diameter D_m and total number concentration N_t (Fig. 3.3).

Very encouraging results were obtained if the microphysical retrievals are performed with the dedicated ground-based polarimetric radars that track the aircraft using a specially designed

scanning strategy. Blanke et al. (2022) tested our retrieval algorithms using the polarimetric

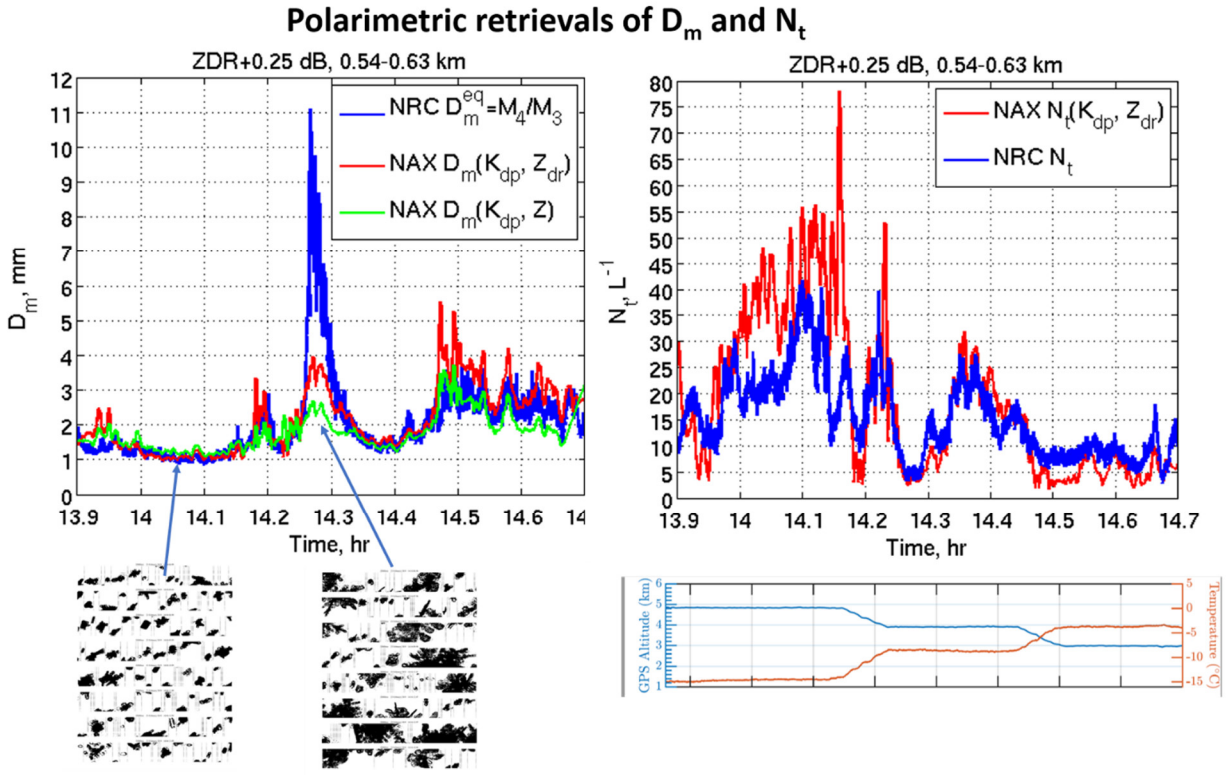

Fig. 3.3. *Polarimetric retrievals of the mean volume diameter D_m and total number concentration N_t of ice crystals during the Convair 580 ICICLE flight on 23 February 2019. Blue curves depict in situ microphysical measurements whereas red and green curves indicate results of polarimetric retrievals with the airborne X-band radar.*

Doppler on Wheels (DoW) mobile radar during the Olympic Mountain Experiment (OLYMPEX). Vertical profiles of the retrieved microphysical variables were derived from the sector-averaged RHIs in the azimuthal sector containing the University of North Dakota (UND) Citation instrumented aircraft. The results of comparison of the retrieved and directly measured microphysical variables are illustrated in Fig. 3.4. Overall good agreement between the measured and retrieved values of IWC, D_m, and N_t is quite encouraging.

It was demonstrated in the studies by Murphy et al. (2020) and Dunnavan et al. (2022) that operational WSR-88D radars can also be effectively used for validation of the radar microphysical retrievals in ice. Such an opportunity was first explored during the DOE Midlatitude Continental Convective Clouds Experiment (MC3E) in 2011. During this experiment, the University of North Dakota (UND) Cessna Citation II aircraft penetrated a number of storms. One of the most valuable in situ microphysical datasets collected onboard an aircraft was obtained during the MCS event on 20 May 2011 which was also observed with several DOE ARM radars and the KVNX WSR-88D radar. The aircraft made spiral ascents and descents from the dendritic growth layer at the temperatures between -10 and -20ºC down to the melting layer (ML) in the stratiform part of MCS

on May 20, 2011. Fig. 3.5 shows a direct comparison of aircraft in situ data (lines) to ice microphysical retrievals (black dots) performed on moving CVP data.

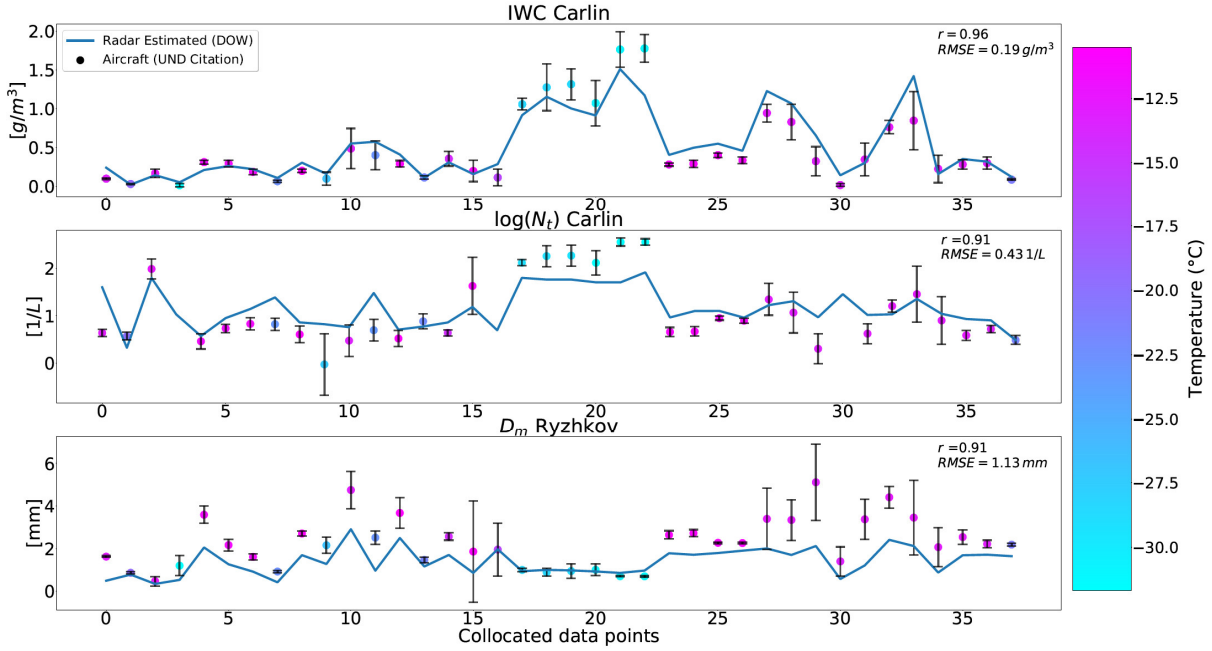

Fig. 3.4. *Co-located aircraft in situ data in chronological order (colored dots) and the best performing set of ice microphysical retrievals based on DoW data (solid blue lines) for 10 flight missions during OLYMPEX. Plots represent from top to bottom IWC and N_t retrieved using relations from Carlin et al. (2021) and D_m retrieved using the $D_m(Z,K_{DP})$ relation from Ryzhkov and Zrnic (2019). Colors indicate the respective temperatures and vertical bars – standard deviations of the in situ measurements. From Blanke et al. (2022).*

Data are not shown when the aircraft was flying below the ML. Overall, the retrievals estimated particle size fairly well at high altitudes, with D_m retrievals diverging from measurements primarily when the aircraft was near the ML (i.e., near gaps in the plot). Errors in the N_t estimates were higher and the estimates of IWC were predominantly biased low and, like D_m estimates, diverged from measured values when the aircraft was near the ML. In addition, these data and retrievals are compared to other Z-based retrievals for both D_m and IWC. Retrievals of D_m were performed using the $Z - D_m$ relations of Skofronick-Jackson et al. (2019) (panel a, red dots) and Matrosov et al. (2019) (panel a, magenta dots) and the IWC(Z, T) relation of Hogan et al. (2006) (panel c, blue dots). The polarimetric retrievals predict values closer to those measured by the HVPS aircraft probes than the other methods for a large majority of the collocated points.

Dunnavan et al. (2022) further refined the polarimetric retrieval methodology and developed a novel routine for matching the ground-based radar and aircraft measurements using a bootstrapping approach. The data from a multitude of the WSR-88D radars integrated via the Multi Radar Multi Sensor (MRMS) platform (Zhang et al. 2016) have been used for collocation with in

situ P3 aircraft measurements during the Investigations of Microphysics and Precipitation for Atlantic Coast-Threatening Snowstorms (IMPACTS) field campaign in 2020. The use of the

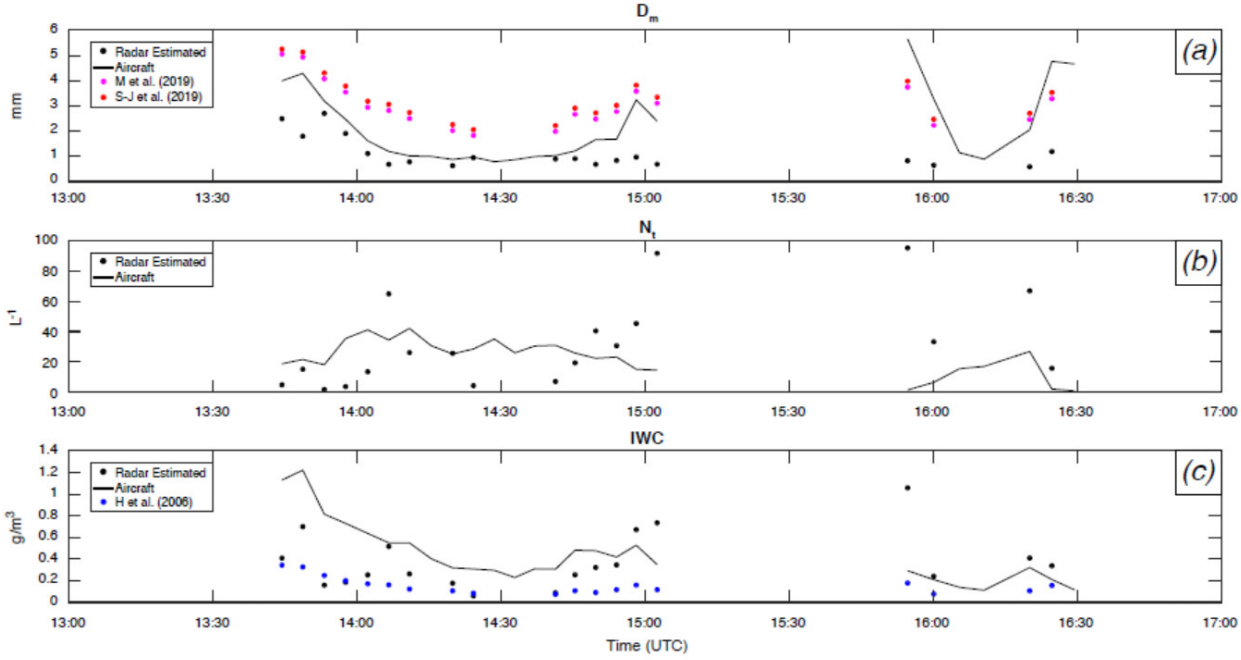

Fig. 3.5. *Collocated aircraft in situ data (solid line) and ice microphysical retrievals of moving CVP data (dots) collected on May 20, 2011. Additional D_m and IWC retrievals by Skofronick-Jackson et al. (2019) (a, red dots), Matrosov et al. (2019) (a, magenta dots), and Hogan et al. (2006) (c, blue dots) using collocated radar data are also shown. Panels are of (a) D_m, (b) N_t, and (c) IWC. Retrievals data shown herein are limited to altitudes above 4.5 km, and data collected below that level are not shown. Units are (a) mm, (b) L^{-1}, and (c) g m^{-3}.*

operational polarimetric radars of opportunity which may not be sufficiently close to the research aircraft and which utilize antenna scanning strategies not optimized for tracking the aircraft inevitably causes a certain mismatch between the radar and in situ measurements. However, such methodology has a universal character and can be utilized for any field experiments involving research aircraft flights within the CONUS area covered by the operational network of the polarimetric WSR-88D radars.

The results of these validation efforts are quite positive although we continue testing and refining the retrieval relations in ice. Nevertheless, at the moment, we have enough confidence in our retrievals to utilize them in our climatological study presented in the next section of the report. These validation studies indicate that the polarimetric retrieval methods successfully passed the feasibility tests, and their products can be used to build a CONUS-wide climatology of the vertical profiles of microphysical parameters in different types of weather systems.

3.3 Climatology of the vertical profiles of polarimetric radar variables and microphysical parameters of ice

A climatology of the vertical profiles of polarimetric radar variables and retrieved microphysical parameters such as LWC/IWC, mean volume diameter D_m, and total number concentration N_t has been documented for the three types of weather systems: continental MCSs, maritime MCSs, and tropical cyclones / hurricanes (Hu and Ryzhkov 2022). This climatology is built based on the analysis of the WSR-88D radar data for 13 continental and 10 maritime MCSs and 11 landfalling hurricanes using the RD-QVP and CVP methodologies. Separate statistics of the vertical profiles have been examined for the high ice water content (HIWC) areas in the storms and compared with their "background" environment. The background statistics encompasses all stratiform parts of the clouds regardless of their ice water content whereas the "HIWC" one is built for the vertical columns in the clouds containing high ice water content above the melting layer with vertically integrated IWC or ice water path (IWP) exceeding a certain threshold. The two statistics require different methodologies for processing of the radar data. The RD-QVP technique is suitable for the first one because the data are analyzed in a 50 km – radius vertical column centered on the radar. The HIWC statistics implies identification and tracking the HIWC areas within the storm which can be farther than 50 km from the radar and estimating vertical profiles in continuously moving columns containing high amount of ice. The CVP methodology is the best choice for this task.

Vertical median profiles of radar variables and retrieved microphysical parameters corresponding to the "background" statistics (no HIWC) for the continental / maritime MCSs and hurricanes are shown in Fig. 3.6. One of the important conclusions from Fig. 3.6 is that continental MCSs are characterized by larger size (D_m) and lower number concentration (N_t) compared to the maritime storms (MCSs and hurricanes) whereas the values of IWC are generally comparable in the two weather systems. Similar median profiles in areas with HIWC are presented in Fig. 3.7. A distinctive feature of the median HIWC profiles is a significant increase of median K_{DP} in ice with a pronounced maximum in the dendritic growth layer (DGL). Such a maximum is particularly strong in the maritime storms. The increase of K_{DP} in DGL is accompanied by strong enhancement of N_t and IWC. The corresponding values of IWC are about three times higher than in the "background" RD-QVP statistics.

An alternative way to summarize the results of our analysis illustrated in Figs. 3.6 and 3.7 is to show a distribution of the median value of IWC in the $\log(N_t) – D_m$ plane. Fig. 3.8 shows that the highest median values of IWC approaching 1.5 – 2 g m^{-3} are observed in the hurricanes and marine MCSs and these are primarily associated with the highest total number concentration of ice N_t and smallest sizes of ice particles D_m. The continental MCSs reveal quite different pattern with noticeably lower median values of IWC even for HIWC cases.

An overarching conclusion of the study is that maritime tropical storms (MCSs and hurricanes) are characterized by smaller size ice in higher concentration compared to the continental MCSs. High ice water content in the HIWC areas is primarily caused by a strong jump in a number concentration of ice particles rather than the increase of their size compared to the "background"

environment. This may point to the homogeneous nucleation of excessive amounts of supercooled droplets and / or secondary ice production as the possible origins of HIWC.

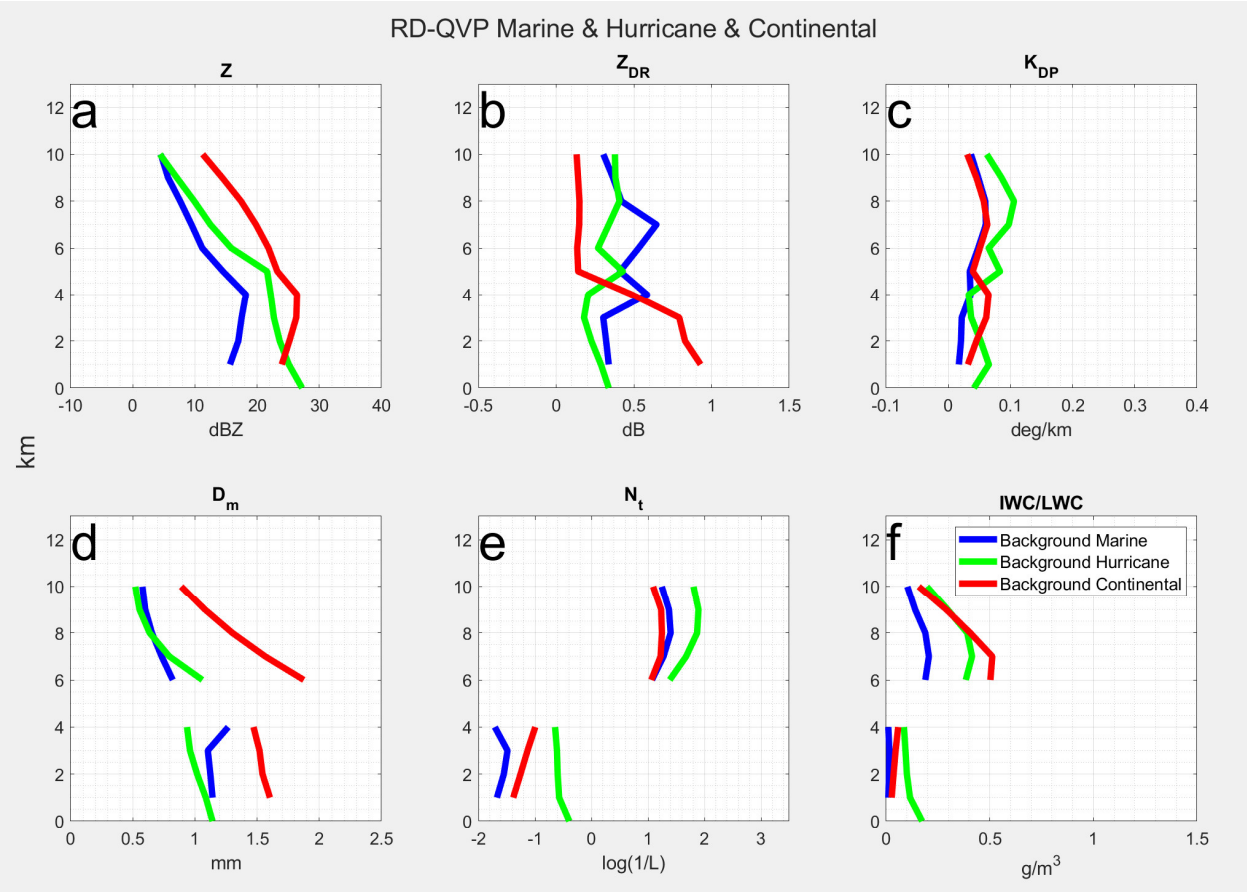

Fig. 3.6. *Median vertical profiles for the RD-QVP "background" dataset: (a) Z, (b) Z_{DR}, (c) K_{DP}, (d) D_m, (e) N_t, and (f) IWC / LWC. Blue, green, and red lines represent marine, hurricanes, and continental profiles, respectively. From Hu and Ryzhkov (2022).*

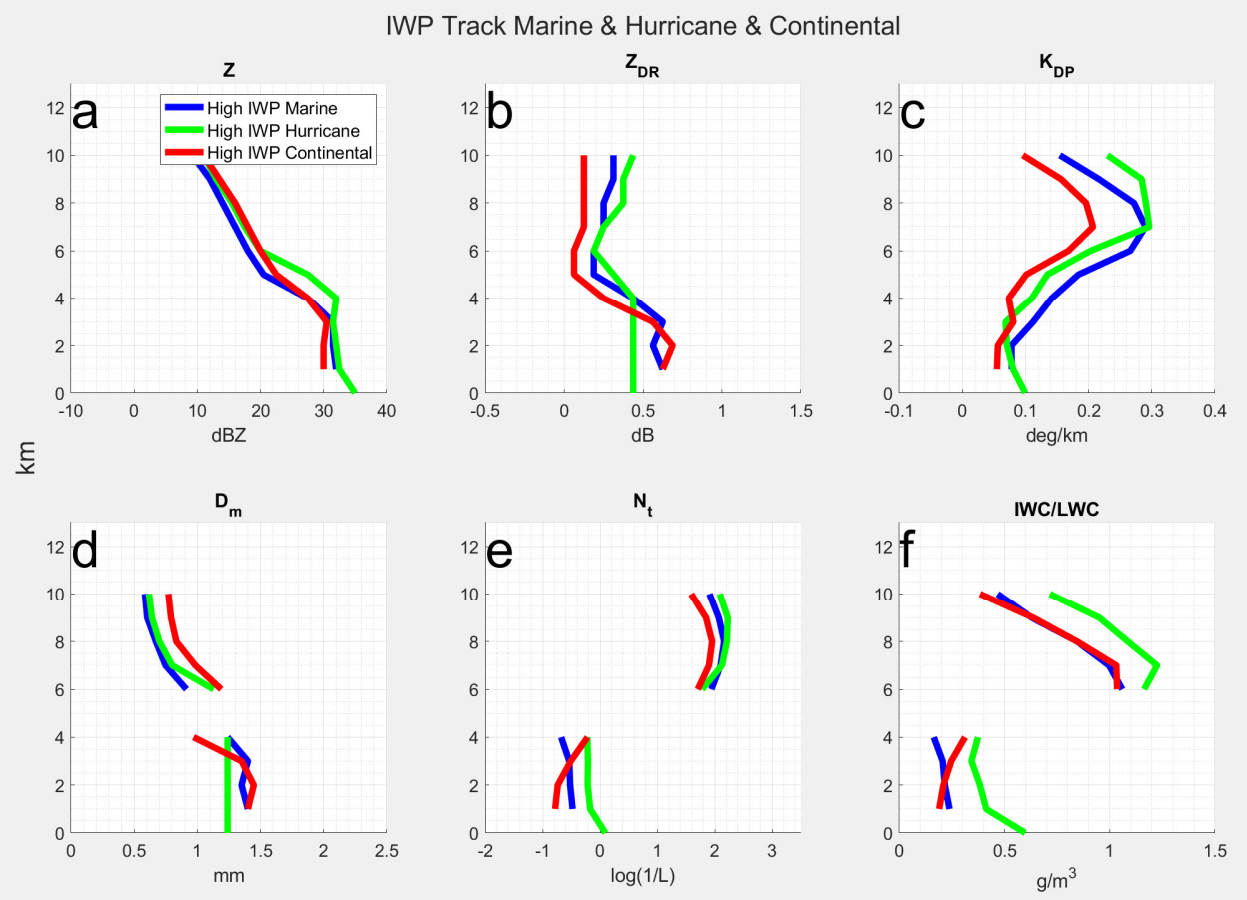

Fig. 3.7. *Median vertical profiles for the CVP "HIWC" dataset: (a) Z, (b) Z_{DR}, (c) K_{DP}, (d) D_m, (e) N_t, and (f) IWC / LWC. Blue, green, and red lines represent marine, hurricanes, and continental profiles, respectively. From Hu and Ryzhkov (2022).*

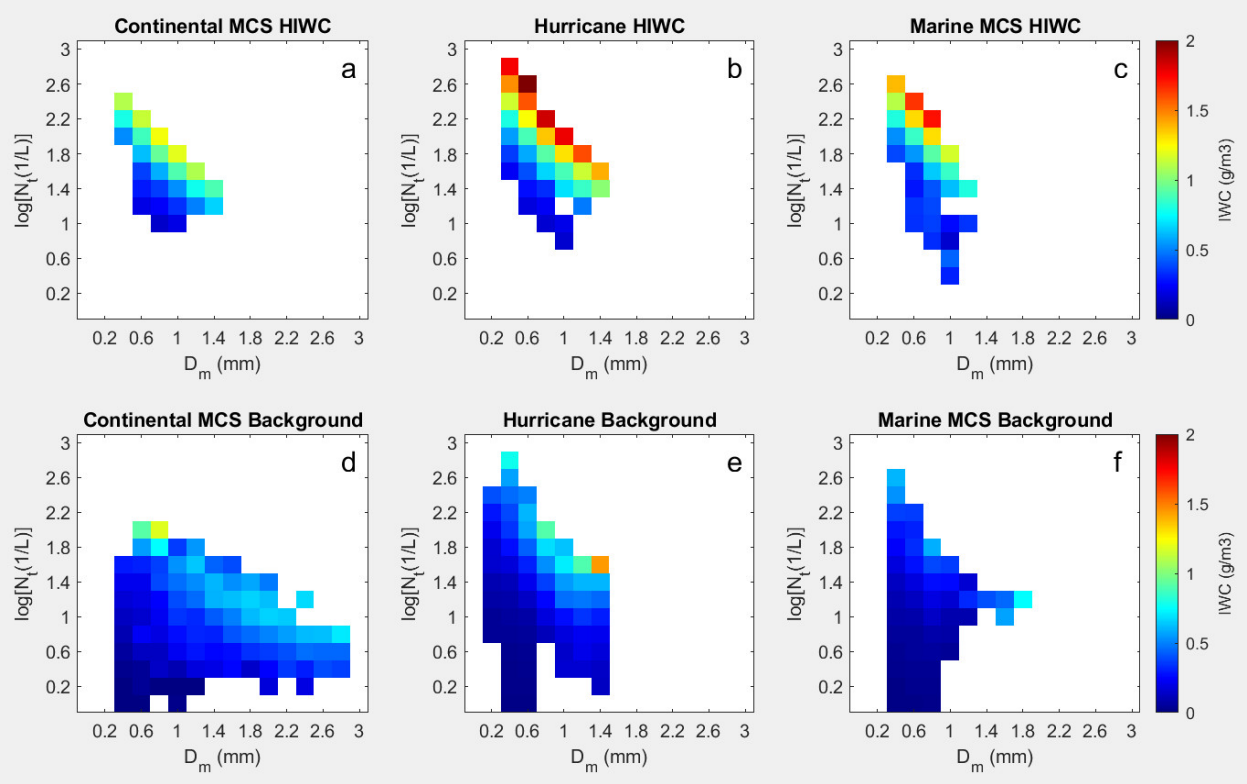

Fig. 3.8. *Distribution of the median values of IWC in the log(N_t) versus D_m plane for the HIWC and background statistics for three types of weather systems ([a] and [d], Continental MCS, [b] an d[d] Hurricane, [c] and [f] Marine MCS).*

Herein, we would like to stress the importance of using operational polarimetric weather radars to complement the utilization of the DOE research radars during dedicated field campaigns to better understand the nature of HIWC because of the continuous global coverage provided by operational NWS radars. A good example of HIWC associated with a marine MCS observed south of the Florida Key West is illustrated in Fig. 3.9 where the fields of Z and K_{DP} are displayed at the altitude of 8.5 km where the temperature is about -25°C. According to the FAA regulations, commercial airplanes have to avoid areas with Z > 20 dBZ to reduce the risk of icing associated with HIWC but can fly freely in areas with Z < 20 dBZ. However, the pockets of K_{DP} exceeding 0.3 – 0.4 °/km or even 0.7 °/km at Z < 20 dBZ visible in the K_{DP} panel definitely indicate HIWC regions with IWC well above 1 g m^{-3} and reaching 2.3 g m^{-3} in a couple of spots. This is a classical maritime situation where several relatively weak convective cells are capable to produce HIWC in their proximity and beyond.

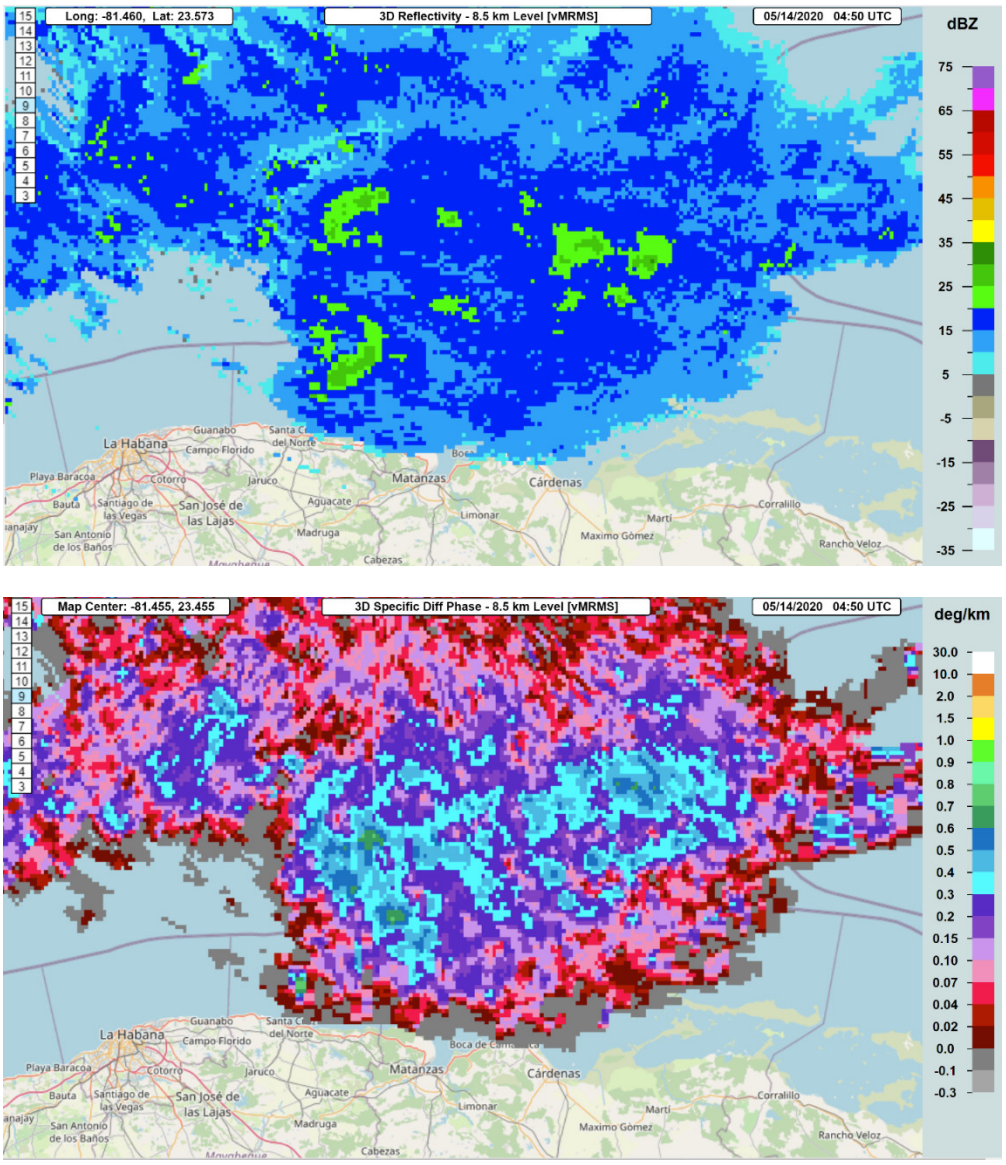

Fig. 3.9. *The fields of Z (top panel) and K_{DP} (bottom panel) at the altitude of 8.5 km (T = -25°C) associated with marine MCS observed by the Key West WSR-88D radar on 14 May 2020. The HIWC areas with Z < 20 dBZ are evident in the K_{DP} panels where K_{DP} > 0.3 – 0.4 °/km.*

3.4 References for section III (the papers supported by this DOE grant are highlighted in blue)

Blanke, A., Heymsfield, A., Moser, M., and Trömel, S.: Evaluation of state-of-the-art polarimetric ice microphysical retrievals exploiting ground-based radar and airborne in-situ measurements, EGU General Assembly 2022, Vienna, Austria, 23–27 May 2022, EGU22-7623, https://doi.org/10.5194/egusphere-egu22-7623, 2022.

Bukovčić, P., A. Ryzhkov, D. Zrnić, and G. Zhang, 2018: Polarimetric radar relations for quantification of snow based on disdrometer data. *J. Appl. Meteor. Climatol.,* **57**, 103–120.

Bukovčić, P., A. Ryzhkov, and D. Zrnić, 2020: Polarimetric relations for snow estimation--radar verification. *J. Appl. Meteor. Climatol.,* **59**, 991–1009.

Dunnavan, E., J. Carlin, J. Hu, P. Bukovcic, A. Ryzhkov, G. McFarquhar, J. Finlon, S. Matrosov, and D. Delene (2022) Radar retrieval evaluation and investigation of dendritic growth layer polarimetric signatures in a winter storm. *Journal of Applied Meteorology and Climatology*, 61, 1679–1705.

Hogan, R., M. Mittermaier, and A. Illingworth, 2006: The retrievals of ice water content from radar reflectivity factor and temperature and its use in evaluating a mesoscale model. *J. Appl. Meteorol. Climatol.*, **45**, 301 – 317.

Homeyer, C., A. Fierro, B. Schenkel, A. Didlake, G. McFarquhar, A. Ryzhkov, J. Basara, A. Murphy, J. Hu (2021) Polarimetric signatures in landfalling tropical cyclones. *Monthly Weather Review*, **149**, 131–154.

Hu, J., and A. Ryzhkov (2022) Climatology of the vertical profiles of polarimetric radar variables and retrieved microphysical parameters in continental / tropical MCSs and landfalling hurricanes. *Journal of Geophysical Research: Atmospheres*, **127**, e2021JD035498.

Matrosov, S., A. Ryzhkov, J. Hardin, M. Shupe, M. Maahn, G. de Boer, and T. Uttal, 2019: Intercomparison of CloudSat and ground-based radar measurements during satellite overpasses. *39th Conf. on Radar Meteorology*, Nara, Japan, Amer. Meteor. Soc., 11A-02.

Murphy, A., A. Ryzhkov, and P. Zhang (2020) Columnar Vertical Profiles (CVP) methodology for validating polarimetric radar retrievals in ice using in situ aircraft measurements. *Journal of Atmospheric and Oceanic Technology*, 37, 1623–1642.

Nguyen, C., M. Wolde, and A. Korolev (2019) Determination of ice water content (IWC) in tropical convective clouds from X-band dual-polarization airborne radar. *Atmospheric Measurement Techniques*, 12, 5897–5911.

Ryzhkov, A., D. Zrnic, and B. Gordon, 1998: Polarimetric method for ice water content determination. *J. Appl. Meteor.*, **37**, 125 – 134.

Ryzhkov, A., P. Zhang, H. Reeves, M. Kumjian, T. Tschallener, C. Simmer, S. Troemel (2016) Quasi-vertical profiles – a new way to look at polarimetric radar data. *Journal of Atmospheric and Oceanic Technology,* 33, 551–562.

Ryzhkov, A., Pinsky, M., Pokrovsky, A., & Khain, A. (2011). Polarimetric radar observation operator for a cloud model with spectral microphysics. *Journal of Applied Meteorology and Climatology*, *50*(4), 873–894.

Ryzhkov, A., and D. Zrnic, 2019: *Radar Polarimetry for Weather Observations*. Springer, 486 pp.

Ryzhkov, A., J. Snyder, J. Carlin, A. Khain, and M. Pinsky, 2020: What polarimetric weather radars offer to cloud modelers: Forward radar operators and microphysical / thermodynamic retrievals. *Atmosphere*, **11**, 362; doi:10.3390/atmos11040362, 34 pp.

Skofronick-Jackson, G., M. Kulie, L. Milani, J. Munchak, N. Wood, and V. Levizzani, 2019: Satellite estimation of falling snow: A Global Precipitation Measurement (GPM) Core Observatory perspective. *J. Appl. Meteorol. Climatol.*, **58**, 1429 – 1448.

Tobin, D., and M. Kumjian, 2017: Polarimetric radar and surface-based precipitation-type observations of ice pellet to freezing rain transitions. *Weather and Forecasting*, **32**, 2065–2082.

Zhang, J. and Coauthors, 2016: Multi-Radar Multi-Sensor (MRMS) quantitative precipitation estimation: Initial operating capabilities. *Bull. Amer. Meteor. Soc.,* **97**, 621–638.

IV Discussion and conclusions

Cloud modeling studies have been performed by the research teams at The Hebrew University of Jerusalem (HUJ) and Lund University to identify the origins of high concentrations of cloud ice in areas of high ice water content (HIWC). The Hebrew University Cloud Model (HUCM) with full spectral bin microphysics and the Lund University aerosol-cloud (AC) model with a hybrid bin / bulk microphysics scheme complementing HUCM were utilized for simulations. The HUCM model demonstrated good skills in reproducing quite realistic size distributions of raindrops and ice crystals as well as radar signatures of the melting layer. Both research teams had particular focus on secondary ice production (SIP) as one of the possible sources of enhanced ice concentration.

The HUJ group suggested a novel concept of ice multiplication during droplet freezing. It is assumed that splintering and droplet fragmentation during droplet freezing takes place because of dendritic growth within a supercooled drop. The resulting simulations of SIP generated small ice in concentrations exceeding hundreds per liter similar to what was observed in the HIWC regions of the tropical storms.

The Lund team explored the SIP mechanisms such as breakup of ice particles due to ice-ice collisions and ice sublimation that are expected to dominate the continental storms. They also quantified the impact of homogeneous nucleation of cloud droplets on the total number concentration of ice at very low temperatures near the tops of the clouds. Additionally, the Lund AC model is able to simulate the effect of aerosols of various types (including biological) on the cloud life cycle and the corresponding ice production.

It is demonstrated that the impact of the primary biological aerosol particles as ice nuclei (PBAP-IN) is expected to be relatively minor (at least for continental storms). The models predict the overall ice enhancement (IE) by SIP up to 10^3 - 10^4 at lower altitudes above the melting layer (ML) and homogeneous freezing supercooled liquid droplets prevails in overall ice concentrations in the upper half of the mixed-phase region in stratiform regions of the storm.

The polarimetric forward radar operator developed by the University of Oklahoma team was used to convert the model output into the fields of radar variables such as radar reflectivity Z and specific differential phase K_{DP}. The simulated vertical profiles of ice water content (IWC), total number concentration (N_t), and the corresponding Z and K_{DP} were compared with the ones directly measured by in situ microphysical probes onboard research aircraft and estimated with the ground-based polarimetric radar for the storm on 20 May 2011 during the DOE MC3E campaign. For the first time, the shape of the vertical profile of K_{DP} was realistically reproduced by the cloud model with the K_{DP} maximum in the dendritic growth layer (DGL) centered at the -15°C isotherm.

The study at the University of Oklahoma demonstrated an extremely important role of K_{DP} for reliable quantification of ice because it is approximately proportional to the first moment of the size distribution of ice and N_t. In the course of the project, the polarimetric radar retrievals of IWC, N_t, and the mean volume diameter D_m developed at the University of Oklahoma have been validated using in situ aircraft measurements during 6 field campaigns and proved to be quite robust and reliable. This allowed us to build the first climatology of the vertical profiles of

polarimetric radar variables and retrieved microphysical parameters for the three types of weather systems: continental MCSs, maritime MCSs, and tropical cyclones / hurricanes (Hu and Ryzhkov 2022). The data were collected by a multitude of the WSR-88D radars in 13 continental and 10 maritime MCSs and 11 landfalling hurricanes. The HIWC areas were identified within the examined storms and the corresponding "HIWC statistics" was compared with the "background" one without HIWC. An overarching conclusion of the study is that maritime tropical storms (MCSs and hurricanes) are characterized by smaller size ice in higher concentration compared to the continental MCSs. High ice water content in the HIWC areas is primarily caused by a strong jump in a number concentration of ice particles rather than the increase of their size compared to the "background" environment. This may point to the homogeneous nucleation of excessive amounts of supercooled droplets and / or secondary ice production as the possible origins of HIWC.

Such a climatology provides a good observational reference for the modelers to evaluate the performance of their models. As an example, the in-depth analysis of the 20 May 2011 MC3E case shows that the advanced cloud models developed in the course of this study still tend to underestimate the number concentration of ice in the HIWC areas although they succeed in reproducing realistically looking vertical profiles of IWC and $N_{t.}$ (Patade et al. 2022).

The results of the project research are summarized in 13 journal papers.